

1 **Loss of nitrogen via anaerobic ammonium oxidation (anammox) in** 2 **the California current system during the late Quaternary**

3 Zoë R. van Kemenade¹, Zeynep Erdem¹, Ellen C. Hopmans¹, Jaap S. Sinninge Damsté^{1,2}, Darci Rush¹

4 ¹ NIOZ Royal Netherlands Institute for Sea Research, PO Box 59, 1790 AB, Den Burg, The Netherlands

5 ² Department of Earth Sciences, Utrecht University, Princetonlaan 8a, 3584 CB, Utrecht, the Netherlands

6 *Correspondence to:* Zoë R. van Kemenade (zoe.van.kemenade@nioz.nl)

7 **Abstract.** The California current system (CCS) hosts one of the largest oxygen minimum zones (OMZs) in the world: the
8 Eastern North Pacific (ENP) OMZ, which is dissociated into a subtropical and tropical region (i.e., the ESTNP and ETNP).
9 In the modern ENP OMZ, bioavailable nitrogen (N) is lost via denitrification and anaerobic ammonium oxidation
10 (anammox). Even so, paleo-reconstructions of N-loss have focused solely on denitrification. Fluctuations in bulk
11 sedimentary $\delta^{15}\text{N}$ over glacial-interglacial cycles have been interpreted to reflect variations in denitrification rates in
12 response to ETNP OMZ intensity changes. This $\delta^{15}\text{N}$ signal is thought to be transported northwards to the ESTNP OMZ.
13 Here, we present the first CCS sedimentary record of ladderane lipids, biomarkers for anammox, located within the ESTNP
14 OMZ (32°N; 118°W). Over the last two glacial terminations (~160 cal ka BP), ladderane concentrations were analysed in
15 combination with the index of ladderanes with five cyclobutane moieties (NL₅), short-chain (SC) ladderane degradation
16 products, and productivity proxies. This shows that: 1) ladderanes derived from anammox bacteria living within the ESTNP
17 OMZ water column; 2) ladderanes were continuously present, with relatively high concentrations during both glacial- and
18 interglacial-periods, showcasing the ESTNP OMZ must have retained an anoxic core in which N-loss occurred; and 3)
19 anammox abundance appears to have been driven both by OM-remineralization and advection changes, which regulated
20 nutrient and oxygen levels. Our study shows that anammox was an important feature in the CCS and provides a more holistic
21 picture of N-loss dynamics and the development of the ESTNP OMZ over glacial-interglacial cycles. Lastly, ladderanes and
22 their SC-products were also detected in 160–500 cal ka BP sediments (15.7–37.5 mbsf; analysed at a low temporal
23 resolution), highlighting their potential as anammox biomarkers in relatively deeper buried sediments for future studies.

24 **1 Introduction**

25 The California current system (CCS) is one of four major Eastern Boundary upwelling systems (EBUS). In EBUS, wind-
26 driven offshore advection of surface waters causes deeper, cold, nutrient-rich waters to be upwelled into the photic zone,
27 fuelling primary productivity (e.g., Bakun and Nelson, 1991). Consequently, the CCS is one of the world's most productive
28 oceanic regions, with year-round upwelling, resulting in high primary production rates (Huyer, 1983; Dorman and Winanat,
29 1995). In the CCS, the respiration of sinking organic matter (OM), in combination with limited ventilation of the North
30 Pacific intermediate waters (Reid and Mantyla, 1978; Sonnerup et al., 1999; Fine et al., 2001), results in the formation of the

31 Eastern North Pacific oxygen minimum zone (ENP OMZ). The ENP is divided into the Eastern tropical North Pacific
32 (ETNP; ~~0–25°N; 75–180°W~~) and Eastern subtropical North Pacific (ESTNP; ~~25–52°N; 75–180°W~~) OMZs.

33 The suboxic/anoxic conditions of OMZs cause the marine nitrogen (N) cycle to shift towards two processes that
34 result in the loss of bioavailable N through the production of dinitrogen gas (N₂): 1) anaerobic ammonium oxidation
35 (anammox) and 2) denitrification. Anammox is the oxidation of ammonium (NH₄⁺) to N₂ using NO₂⁻ as the terminal electron
36 acceptor (van de Graaf et al., 1997, 1995), and is performed in the marine water column by anammox bacteria of the genus
37 ‘*Ca. Scalindua*’ (Kuypers et al., 2003). Anammox bacteria are chemolithoautotrophs and use carbon dioxide (CO₂) as their
38 carbon source. Denitrification is the stepwise reduction of nitrate (NO₃⁻), to nitrite (NO₂⁻), to N₂ (Kuenen and Robertson,
39 1987) and is performed by a wide range of organisms, most of which are heterotrophs. During denitrification, nitrous oxide
40 (N₂O) can be released as an intermediate product (Kuenen and Robertson, 1987), which has a global warming potential 265
41 times that of CO₂ (Vallero, 2019).

42 While permanent OMZs contribute to only 8 % of the total oceanic area (Paulmier and Ruiz-Pino, 2009), they are
43 responsible for 20–50 % of total global N loss (Gruber, 2004; Codispoti et al., 2001). Decreased N availability in OMZs may
44 limit primary producers, and hence, the uptake of CO₂ into the organic matter (OM) pool. This may reduce the efficiency of
45 the ocean’s biological pump, which exports organic C from the euphotic zone to the sea floor. Thus, OMZs not only have a
46 disproportionately large impact on the marine nitrogen cycle, but changes in N-loss dynamics may also feed back into the
47 carbon cycle.

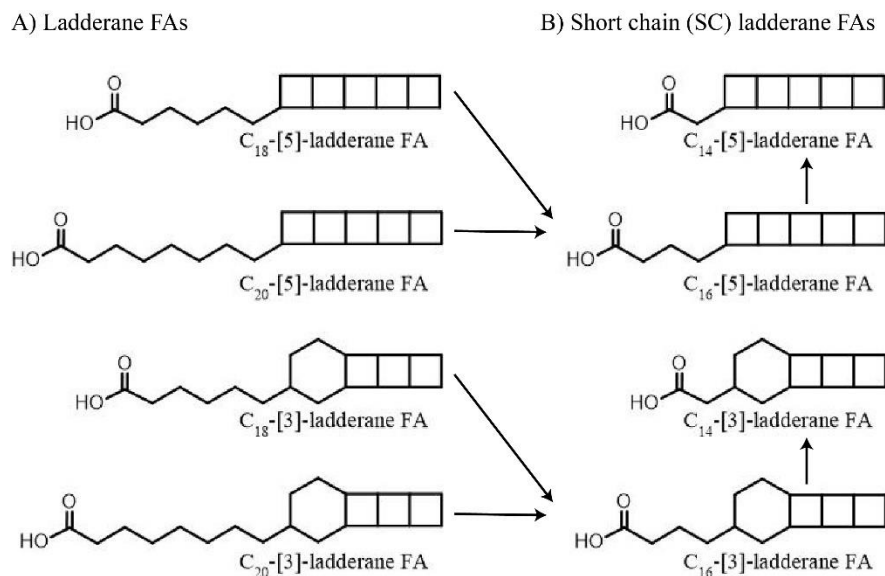
48 The ENP OMZ is expanding both vertically (shoaling towards the ocean’s surface; Bograd et al., 2008) and
49 horizontally (Zhou et al., 2022) with present-day climate change. This follows observed trends of overall deoxygenation of
50 the North Pacific since the 1960’s (Whitney et al., 2007; Stramma et al., 2010; Pierce et al., 2012; Smith et al., 2022), linked
51 to anthropogenically-induced ocean warming as a response to increased greenhouse gas emissions (Laffoley and Baxter,
52 2019). As a result of the decreasing dissolved oxygen (DO) concentrations, denitrification has been shown to increase in the
53 North Pacific over the last decades (Peters et al., 2018; White et al., 2019). Vertical expansion and intensification of the ENP
54 OMZ have also occurred in the absence of anthropogenic influences in the past, as recorded by redox-sensitive trace metals
55 in the sedimentary archive (Wang et al., 2020). This is thought to be caused by changes in DO concentrations during glacial-
56 interglacial transitions (terminations). Model simulations indicate that during glacials, cooling of the polar regions led to a
57 more restrained and intensified Hadley cell (Nicholson and Flohn, 1981). This is thought to have caused southward transport
58 of high-oxygen, nutrient-rich North Pacific Intermediate Water (NPIW; Herguera et al., 2010) and limited northward
59 advection of the warm, oxygen-poor California undercurrent (CU; ~~Fig. 21~~), resulting in a more oxygenated OMZ. During
60 interglacials, the oxygen deficiency in the OMZ is thought to have increased due to enhanced advection of the warm,
61 oxygen-depleted waters of the CU originating from the tropics ((Lembke-Jene et al., 2018; Hendy and Kennett, 2003), water

62 column stratification (Wang et al., 2020), and enhanced upwelling of nutrient-rich waters (Choumilin et al., 2019). These
63 previous glacial-interglacial transitions may be considered as analogues for the effect of future climate change on the N-
64 cycle.

65 In the CCS, enriched isotope ratio values of bulk sedimentary nitrogen ($\delta^{15}\text{N}$) during interglacial periods have been
66 interpreted to reflect increased denitrification in response to OMZ intensification (e.g., Kienast et al., 2002; Kemp et al.,
67 2003; Liu et al., 2005). Sedimentary $\delta^{15}\text{N}$ values are governed by the isotopic fractionation (ϵ) induced by biological
68 transformations and can be used to infer past N-cycling. For water column denitrification, the production of N_2 induces an
69 isotope fractionation effect of +20 to +30 ‰ on the residual nitrogen (Ryabenko, 2013; Sigman and Fripiat, 2019).
70 Enrichment cultures of anammox bacteria have, however, ~~recently shown that they *Ca. Scalindua* spp. also induces~~induce a
71 similar~~an~~ isotope fractionation effect (Brunner et al., 2013), with that of *Ca. Scalindua* spp. being of +16 to +30 ‰
72 (Kobayashi et al., 2019). Although anammox occurs in the modern North Pacific oxygen deficient waters (Rush et al.,
73 2012a; Peng et al., 2015; Sollai et al., 2015; Hamasaki et al., 2018), and anammox is reported to be the dominant N-loss
74 process in the Eastern Tropical South Pacific (ESTP; Galán et al., 2009; Thamdrup et al., 2006; Hamersley et al., 2007), to
75 the best of our knowledge, there are no reconstructions on the occurrence of anammox in the sediment archive of the CCS.
76 Moreover, a long-standing conundrum is the discrepancy between the timing of enriched $\delta^{15}\text{N}$ values, and enhanced marine
77 productivity, especially north of the ETNP (Kienast et al., 2002), suggesting a decoupling between remineralization rates and
78 N-loss (Ganeshram et al., 2000), ~~(Ganeshram et al., 2000).~~

79 While sedimentary $\delta^{15}\text{N}$ values are shaped by the sum of N-cycling processes, lipid biomarkers provide more
80 detailed information (see Rush and Sinninghe Damsté, 2017 for a review). Anammox bacteria biosynthesise C_{18} and C_{20}
81 ladderane fatty acids (FAs) (Fig. 1)2). These unique lipids contain three or five linearly concatenated cyclobutane rings ([3]-
82 ladderane and [5]-ladderane, respectively; Sinninghe Damsté et al., 2002). Ladderanes have been successfully applied to
83 trace abundances of *Ca. Scalindua* spp. in the modern ENP water column (Rush et al., 2012a; Sollai et al., 2015) and as
84 anammox biomarkers in sedimentary records up to 140 ka (Jaeschke et al., 2009; Rush et al., 2019; van Kemenade et al.,
85 2023). Moreover, during exposure to oxic conditions ladderane FAs undergo microbially-mediated oxic degradation of the
86 alkyl side chain by β -oxidation, in which C_{18} - and C_{20} -ladderane FAs are sequentially transformed into the short-chain (SC)
87 C_{16} - and C_{14} -ladderane partial degradation products (Rush et al., 2011, 2012b). Thus, SC-ladderane FAs in the sediment
88 archive may be used to trace back anammox cell material that has been exposed to oxic conditions, such as sedimentation
89 through the oxic water underlying an OMZ. Furthermore, the index of ladderane FAs with five cyclobutane rings (NL_5) has
90 been shown to correlate with the *in situ* water temperature at which ladderane FAs are synthesised (Rattray et al., 2010),
91 which has been used to determine the provenance of ladderane lipids (Jaeschke et al., 2009; Rush et al., 2012a; Van
92 Kemenade et al., 2022).

93 Here, we describe the occurrence of ladderane FAs in a ~160 cal ka BP sediment record from the CCS, covering the
 94 two most recent glacial terminations (T1 and T2). We combined (SC-)ladderanes and the NL₅ index with sedimentary bulk
 95 $\delta^{15}\text{N}$, stable carbon isotope ratio ($\delta^{13}\text{C}$), total organic C (TOC) and total N (TN) to investigate the feedback of changing
 96 OMZ intensity on the occurrence of anammox within the CCS. Moreover, ladderane FAs were also investigated, albeit in
 97 low-resolution, in >160 cal ka BP sediments (up to 500 cal ka BP) to explore their preservation potential.



99 **Figure 1:** Structures of anammox lipid biomarkers used in this study: A) ladderane fatty acids (FAs) with 5 or 3 cyclobutane moieties
 100 containing 18 or 20 carbon atoms. B) short chain ladderane fatty acids (FAs) with 5 or 3 cyclobutane moieties containing 16 or 14 carbon
 101 atoms. Proposed diagenetic pathways are indicated using black arrows (adapted from Rush et al., 2011).

102 2 Hydrographic setting

103 The northern boundary of the CCS is at the transition zone between the North Pacific Current (NPC) and Alaska gyres
 104 (~50°N) and is bordered in the south by the subtropical waters of Baja California, Mexico (~15–25°N). The CCS (Fig. 2A) is
 105 shaped by: (i) the equatorward California current (CC), extending roughly 1000 km off the North American coast (Checkley
 106 and Barth, 2009), (ii) the poleward, near-shore flowing ~~California undercurrent (CU)CU~~, and (iii) the seasonal poleward
 107 flowing Davidson current (DC). The CC is a year-round, cold, low-salinity, nutrient-rich surface current (<300 m below sea
 108 surface; mbss), originating from the North Pacific Current. While the CC is strongest in spring and summer, the DC
 109 originating around Point Conception (35°N) dominates the surface-flow throughout winter. The deeper waters of the CC are
 110 shaped by the NPIW (300–800 mbss), which circulates clockwise in the North Pacific gyre (Sverdrup et al., 1942) and is
 111 carried southwards by the CC. Around Baja California, it convolutes with unventilated intermediate waters of tropical origin,
 112 which have been transported to the eastern Pacific by the Equatorial undercurrent (EUC; Reid, 1997; Reid and Mantyla,
 113 1978). Here, part of the CC turns north to become the ~~California undercurrent (CU)CU~~. The CU (~100–300 mbss) carries

114 the warm, high-salinity, low oxygen waters from Baja California towards Vancouver Island (Thomson and Krassovski,
115 2010). Within the CCS, the geostrophic flow of the CC in combination with Ekman transport and eddy activity cause an
116 offshore transport of (sub-)surface waters and strong coastal jets, which are replaced by the upwelling of the nutrient-rich
117 undercurrent waters (Huyer, 1983; Chavez and Messié, 2009). Upwelling occurs year-round, and results in high primary
118 production (Bograd et al., 2009). In the CCS, the high organic matter flux, together with the poor ventilation of the
119 intermediate-water mass (Reid and Mantyla, 1978; Fu et al., 2018), results in the formation of the ENP OMZ, disassociated
120 in the ETNP (0–25°N; 75–180°W) and ESTNP (25–52°N; 75–180°W) (Fig. 2B). Dissolved oxygen (DO) concentrations in
121 the cores (<20 $\mu\text{mol kg}^{-1}$) of both the ETNP (~320–740 meters below sea surface, ‘mbss’) and ESTNP (~850–1080) OMZ
122 decrease below <1 $\mu\text{mol kg}^{-1}$ (Palmier and Ruiz-Pino, 2009) (Fig. 2C).

123 3 Methods

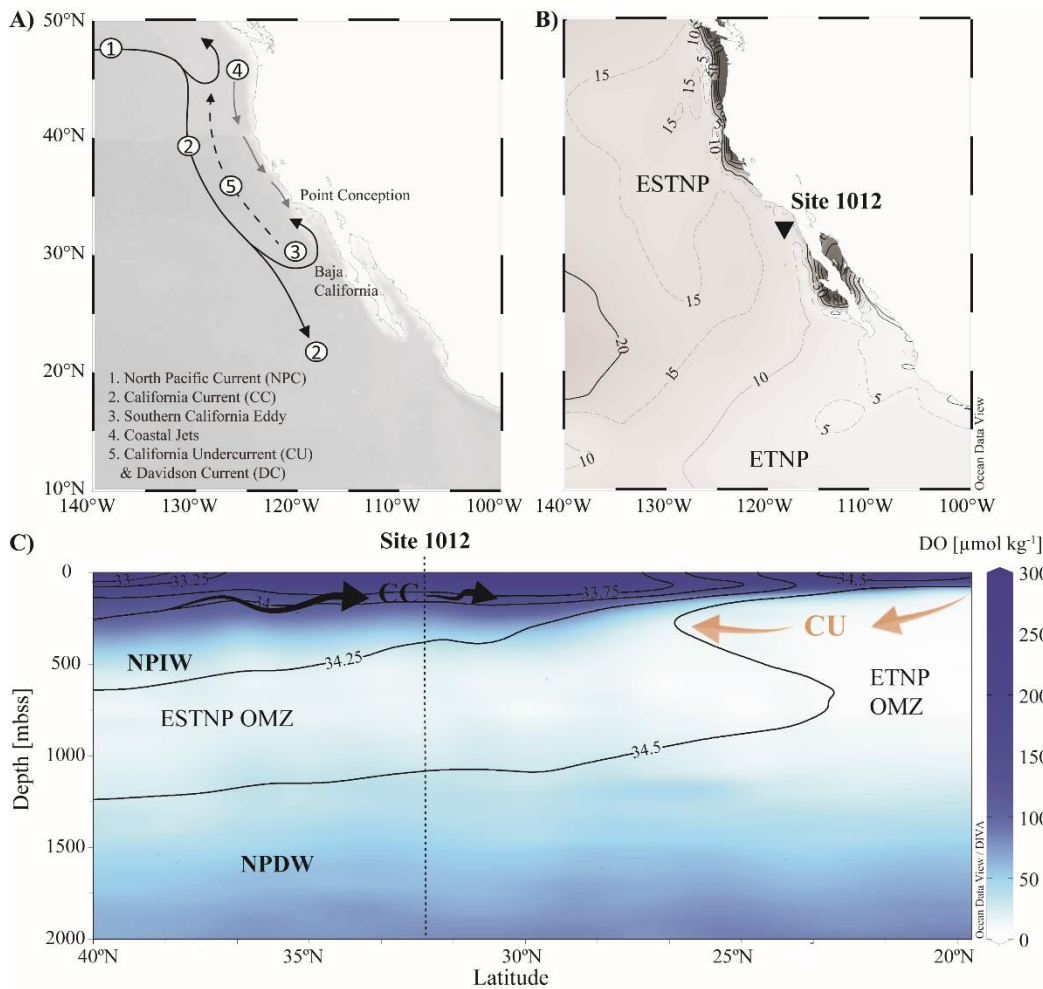
124 3.1 Sampling location and strategy

125 The sediment record was recovered in 1996 during Ocean Drilling Program (ODP) Leg 167 (Lyle et al., 1997) . Site 1012 is
126 located 105 km offshore California in the East Cortez Basin (32°16.970'N, 118°23.039'W), near the southern front of the
127 CC and northern front of the ETNP OMZ (Fig. 2B). The core was recovered from a water depth of 1784 m below sea surface
128 (mbss). For this study, 69 sediment depths (volumes of 20 cm^3) were selected for ladderane FAs analysis. Sedimentation
129 rates ranged from 4 to 15 cm kyr^{-1} (S1, Table 1). Considering the oldest detected ladderane FAs were in 140 ka BP
130 sediments (~10 m below sea floor ‘mbsf’) of the Arabian Sea (Jaeschke et al., 2009), we subsampled at a higher resolution
131 (every 10 to 50 cm) to the first ~160 kyr (15.7 mbsf) of the record (with a maximum resolution of 10 cm around T1 and T2)
132 and at a lower resolution (80 to 200 cm) to ~500 cal ka BP (37.5 mbsf). In addition, 74 sediments (10-50 cm resolution) were
133 analysed for bulk sedimentary organic carbon (TOC) and N (TN) content, the C/N ratio (atomic) and bulk isotopic ratio
134 values ($\delta^{15}\text{N}$ and $\delta^{13}\text{C}$). A detailed overview of all samples is given in Supplement 1, Tables 1 and 2. Samples were freeze-
135 dried and stored at -20 °C prior to analysis.

136 3.2 Analysis of sedimentary bulk TOC, TN, C/N, $\delta^{13}\text{C}$ and $\delta^{15}\text{N}$

137 Sediments were freeze-dried and ground to powder. For TOC and $\delta^{13}\text{C}$ analysis, aliquots of bulk sediment were decalcified
138 to remove all carbonates. Samples were first acidified with 2M hydrochloric acid (HCl) and rinsed with distilled water to
139 remove the salts. After the decalcification step, ca. 0.5 mg of dried material was used for the analysis. For TN and stable
140 nitrogen isotope ratio ($\delta^{15}\text{N}$) between 15 and 20 mg of non-decalcified sediment were used. All samples were packed in tin
141 cups and introduced to the Thermo Scientific Flash 2000 elemental analyzer coupled to a Thermo Scientific Delta V
142 Advantage isotope ratio mass spectrometer (EA/IRMS). Results are expressed in standard notation relative to Vienna Pee

143 Dee Belemnite (VPDB) for $\delta^{13}\text{C}$ and relative to air for $\delta^{15}\text{N}$. The precision as determined using laboratory standards
 144 calibrated to certified international reference standards was in all cases $< 0.2\%$. [The sedimentary C/N ratios \(based on total](#)
 145 [organic C and total N\)](#) were [calculated using their atomic mass.](#)



146
 147 **Figure 2:** A) map of the California Current System (CCS). Key currents are indicated with arrows. B) location of ODP site 1012
 148 ($32^{\circ}16.970'\text{N}$; $118^{\circ}23.039'\text{W}$) recovered at 1784 mbss, with minimum dissolved oxygen (DO) concentrations [$\mu\text{mol kg}^{-1}$] detected in the
 149 water column in 2018 (WOA, 2018). C) A latitudinal section plot of the CCS water column showing modern annually averaged DO (μmol
 150 kg^{-1}) concentrations and salinity (psu) concentrations with the color bar and contour lines, respectively (WOA, 2018). Major current and
 151 water masses are also indicated, i.e., the Eastern Tropical and Eastern Subtropical North Pacific (ETNP and ESTNP, respectively) OMZs,
 152 the California Current (CC; black arrows), the California Undercurrent (CU; orange arrows), North Pacific intermediate waters (NPIW)
 153 and North Pacific deep water (NPDW). Maps were created in Ocean Data View and DIVA gridding was applied for interpolation of DO
 154 concentrations (Schlitzer and Reiner, Ocean Data View, 2021).

155 3.3 Age model

156 Liu et al. (2005) previously constructed an age model for ODP site 1012, based on sediments recovered from Hole B. As the
 157 material used in this study is predominantly from Hole A and C, a revised age model was constructed (S1, Table 1). The

158 revised age model for sediments up to 160 cal ka BP (15.7 m composite depth, 'mcd') was created by correlation of the bulk
159 sedimentary $\delta^{15}\text{N}$ record of Liu et al., (2005) with our dataset. Tie points (age vs composite depth) were selected by fine-
160 tuning using QAnalyseries (version 2022). For sediments >160 cal ka BP, which were solely sampled for ladderane FAs at
161 low resolution (i.e. not sedimentary $\delta^{15}\text{N}$), the age model of Liu et al. (2005) is used.

162 **3.4 Ladderane extraction**

163 Homogenized, freeze-dried sediments were extracted using a low temperature - low pressure accelerated solvent extraction
164 (ASE) method, previously described for ladderane extraction in Rush et al. (2012b). Thereafter, aliquots of the total lipid
165 extract were saponified in 2 N potassium hydroxide (in a 96 % MeOH solution) by refluxing for 1 h. After, 2 mL of
166 bidistilled water was added. The saponified extracts were acidified by adjusting the pH to 3 with 2 N hydrochloric acid (in a
167 50 % MeOH solution). Phase separation was induced by adding 2 mL of DCM. The biphasic mixtures were sonicated for 5
168 min and centrifuged for 2 min (3000 rpm). The DCM layers, containing the FAs, were collected. The mixtures were
169 partitioned twice more with DCM, after which the same procedure was applied before collection of the DCM layers. The FA
170 fractions were dried over a sodium sulphate (Na_2SO_4) column. Then, the fractions were methylated with diazomethane to
171 convert FAs into their corresponding fatty acid methyl esters (FAMES) and allowed to airdry overnight to avoid losing the
172 more volatile SC-ladderane FA had they been dried under a stream of N_2 . The methyl esters of the polyunsaturated fatty
173 acids (PUFAs) were removed by eluting the FAME fractions with DCM over a silica impregnated silver nitrate (AgNO_3)
174 column. FAME fractions were dissolved in acetone and filtered over 0.45 mm PTFE filters (4 mm; BGB, USA).

175 **3.5 Ladderane analysis**

176 A commercially available deuterated $\text{C}_{20}[5]$ -PUFA (Reagecon Diagnostics Ltd.) was added as an internal standard to the
177 FAME fractions. FAME fractions were analysed on an Agilent 1290 Infinity I ultra-high performance liquid
178 chromatographer (UHPLC), equipped with a thermostatted auto-injector and column oven, coupled to a Q Exactive Plus
179 Orbitrap MS, with an atmospheric pressure chemical ionization (APCI) probe (Thermo Fischer Scientific, Waltham, MA)
180 operated in positive ion mode. Separation was achieved with a ZORBAX Eclipse XDB C_{18} column (Agilent, 3.0×250 mm,
181 $5 \mu\text{m}$), using MeOH as an eluant (0.4 ml min^{-1}). APCI source settings were set as follows: corona discharge current, $2.5 \mu\text{A}$;
182 source CID, 10 eV; vaporizer temperature, 475°C ; sheath gas flow rate, 50 arbitrary units (AU); auxiliary gas flow rate,
183 30AU; capillary temperature, 300°C ; and S-lens, 50V (van Kemenade et al., 2022). A mass range of m/z 225–380 was
184 monitored (resolution 140,000 ppm), followed by data-dependent MS^2 (resolution 17,500 ppm at m/z 200), in which the 10
185 most abundant masses in the mass spectrum were fragmented successively (stepped normalised collision energy 20, 25, 30).
186 An inclusion list containing the exact masses of $\text{C}_{14-24}[3]$ - and $\text{C}_{14-24}[5]$ -ladderane FAMES was used. Mass chromatograms
187 (within 5 ppm mass accuracy) of the protonated molecules ($[\text{M}+\text{H}]^+$) were used to integrate the detected ladderanes: $\text{C}_{14}[3]$ -,

188 C₁₄[5], C₁₆[5], C₁₈[3]-, C₁₈[5]-, C₂₀[3]- and C₂₀[5]-ladderane FAMES (*m/z* 235.169, 233.154, 261.185, 291.232, 289.216,
189 319.263 and 317.248, respectively), and the internal deuterated C₂₀[5]-PUFA standard (*m/z* 322.279)-. [A detection limit of](#)
190 [30–35 pg injected on-column and a linear response of \(r\(4\) > 0.99\) over approximately 3 orders of magnitude was achieved](#)
191 [\(S1, Table 8a\)](#). Identification of ladderanes was achieved by comparing retention times and spectra with in-house isolated
192 C₂₀[3]- and C₂₀[5]-ladderane FAME standards (Hopmans et al., 2006; Rattray et al., 2008) and with ladderane FAMES in a
193 biomass sample of *Ca. Kuenenia*.

194 Previously, ladderane FAME quantification has been conducted using calibration curves of in-house isolated C₂₀[3]-
195 and [5]-ladderane standard (Hopmans et al., 2006). However, this quantification method does not correct for any variability
196 in ion intensity, due to e.g., matrix effects and/or changes in the instruments functioning. Therefore, we further optimised
197 this quantification method to include a response correction using a commercially available internal standard (deuterated
198 C₂₀[5]-PUFA). At the start of each sequence, calibration curves were made for the C₂₀[3]- and [5]-ladderane standards *and*
199 the deuterated C₂₀[5]-PUFA standard. The relative response of the deuterated C₂₀[5]-PUFA commercial standard in relation
200 to the ladderane FAME standards was determined from the slopes of their calibration curves (giving a relative response
201 factor, i.e. RRF). An RRF of 1.3 was used for [3]-ladderanes, based on the C₂₀[3]-ladderane, and an RRF of 1.2 for the [5]-
202 ladderane, based on the C₂₀[5]-ladderane. Using the RRFs, ladderane FAME concentrations (*C_L*, expressed in µg · g dry
203 weight⁻¹) were calculated as follows:

$$204 \quad C_L = \frac{m_{IS} \left(\frac{A_L}{A_{IS}} \right)}{m_S} \quad [1]$$

205 With *m_{IS}* being the mass (µg) of the added internal standard, *m_S* the dry weigh of extracted sediment (g), *A_L* the integrated
206 peak area of the given ladderane FAME, *A_{IS}* the integrated peak area of the internal standard, and RRF the relative response
207 factor. Ladderane concentrations (including concentrations normalized against gram TOC) are reported in supplement 1
208 (Tables 4 and 5). To compare with previous studies that did not use an internal standard, the established method that uses
209 external calibration curves of three authentic standards (Hopmans et al., 2006; Rush et al., 2012b; Rattray et al., 2010) was
210 also performed (S1, Table 8b; S2.2). [A comparison between both quantification methods is provided in supplementary](#)
211 [material 2 \(section S2.2\)](#).

212 3.6 NL₅ index

213 The index of ladderane lipids with five cyclobutane rings (NL₅) correlates with the temperature at which they were
214 synthesised. The NL₅ index is calculated according to the following equation:

215
$$NL_5 = \frac{C_{20}[5]ladderane\ FA}{C_{18}[5]ladderane\ FA + C_{20}[5]ladderane\ FA} \quad [2]$$

216 The empirical fourth-order sigmoidal relationship between the NL_5 index and temperature is then described by:

217
$$NL_5 = 0.2 + \frac{0.7}{1 + e^{-\frac{T-16.3}{1.5}}} \quad [3]$$

218 with temperature (T) in °C (Rattray et al., 2010).

219 3.7 Degradation rates and constants

220 Ladderane concentrations over the entire record (Fig. 3) were used to calculate ladderane degradation rates, were calculated
 221 using with the following equations for lipid degradation constants and rates (Canuel and Martens, 1996):

222
$$k' = \frac{-\ln \left[\frac{C_t}{C_{t0}} \right]}{t} \quad [4]$$

223 With k' being the first order rate constant (kyr^{-1}), C being the concentration ($\mu\text{g g sediment}^{-1}$) at time t (C_t) and at the initial
 224 time (C_{t0}), and t being the relative time (kyr). Ladderane degradation constants and rates are provided in supplementary
 225 material 1 (Table 7).

226 4 Results

227 4.1 Bulk sedimentary total nitrogen and total organic carbon

228 Bulk sedimentary total nitrogen (TN) ranged between 0.1–0.6 % throughout the record. $\delta^{15}\text{N}$ fluctuated from 5.8 to 10.0 ‰.
 229 An offset of 3 to 4 ‰ was observed between interglacials and glacials, with higher values during interglacials. Sedimentary
 230 total organic carbon (TOC) varied between 1.7–7.4 % throughout the record, whilst its carbon isotopic composition
 231 ($\delta^{13}\text{C}_{\text{TOC}}$) ranged from -23.0 to -21.6 ‰. C_t/N ratios (atomic) ranged from 134 to 2346 (Fig. 4F–J; S1, Table 3).

232 4.2 Ladderane FAs

233 4.2.1 Ladderane FAs concentrations & the NL_5 index

234 The ladderane fatty acids identified in this record were $\text{C}_{18}[5]$ -, $\text{C}_{18}[3]$ -, $\text{C}_{20}[5]$ - and $\text{C}_{20}[3]$ -ladderanes and their diagenetic
 235 products, the SC $\text{C}_{14}[5]$ -, $\text{C}_{14}[3]$ - and $\text{C}_{16}[5]$ -ladderanes. Summed SC-ladderane and ladderane concentrations over the entire
 236 500 ka record were 0.5–33 and 0.1–23 ng g⁻¹ dry weight, respectively (Fig. 3; S1 Table 5). Normalized concentrations over
 237 the 160 ka record ranged as follows: $\text{C}_{14}[5]$ -ladderane 16–158 ng gTOC⁻¹, $\text{C}_{14}[3]$ -ladderane 27–184 ng gTOC⁻¹, $\text{C}_{16}[5]$ -
 238 ladderane 34–198 ng gTOC⁻¹, $\text{C}_{18}[5]$ -ladderane 7–107 ng gTOC⁻¹, $\text{C}_{18}[3]$ -ladderane 4–76 ng gTOC⁻¹, $\text{C}_{20}[5]$ -ladderane 5–79

ng gTOC⁻¹, and C₂₀[3]-ladderane 10–208 ng gTOC⁻¹ (Fig. 4B, C; S1, Table 4). Summed SC ladderane and ladderane concentrations over the entire 500 ka record 0.5–33 and 0.1–23 ng g⁻¹ dry weight, respectively (Fig. 3; S1 Table 5). Concentrations calculated without the use of the internal standard (Hopmans et al., 2006; see section 2.5) are reported in S1 (Table 8b) and were a factor 1.2 and 1.3 lower for [3]-(SC-)ladderanes [5]-(SC-)ladderanes, respectively. Concentrations calculated with the two quantification methods showed a strong positive linear relationship of R² = 0.88 and 0.89 for [3]-(SC-)ladderanes and [5]-(SC-)ladderanes, respectively (Fig. S2.2). –are reported in S1 (Table 8b).–The NL₅ index (eq. [2]) ranged from 0.3 to 0.8 throughout the record. Corresponding NL₅-derived temperatures (eq. [3]) were between 13.1–18.6°C, with highest values observed in >160 cal ka BP sediments (S1, Table 6).

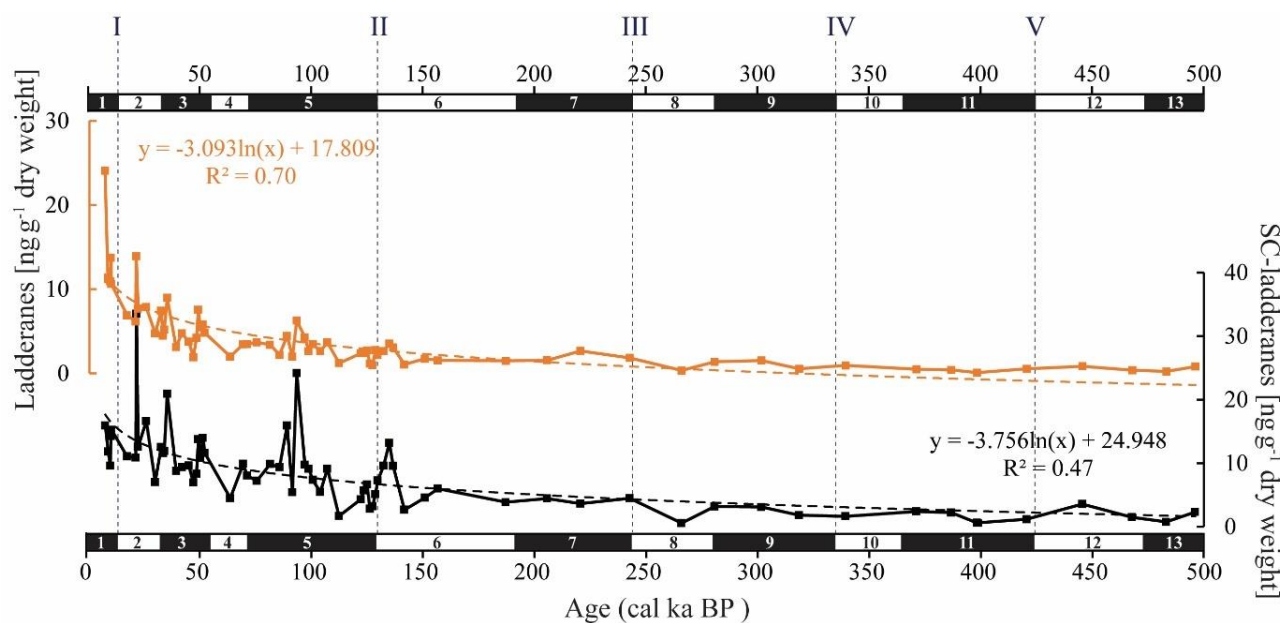


Figure 3: Summed C₁₈[5]-, C₁₈[3]-, C₂₀[5]- and C₂₀[3]-ladderane (orange) and summed short-chain (SC) C₁₄[5]-, C₁₄[3]- and C₁₆[5]-ladderane (black) concentrations (ng g⁻¹ dry weight) in the ODP 1012 record. The logarithmic relationship between ladderanes and SC-ladderanes with time is provided (with corresponding R²), and displayed with orange and black spaced lines, respectively. Grey spaced lines indicate the approximate timing of glacial terminations I to V. N.B. the scales of the y-axes are different.

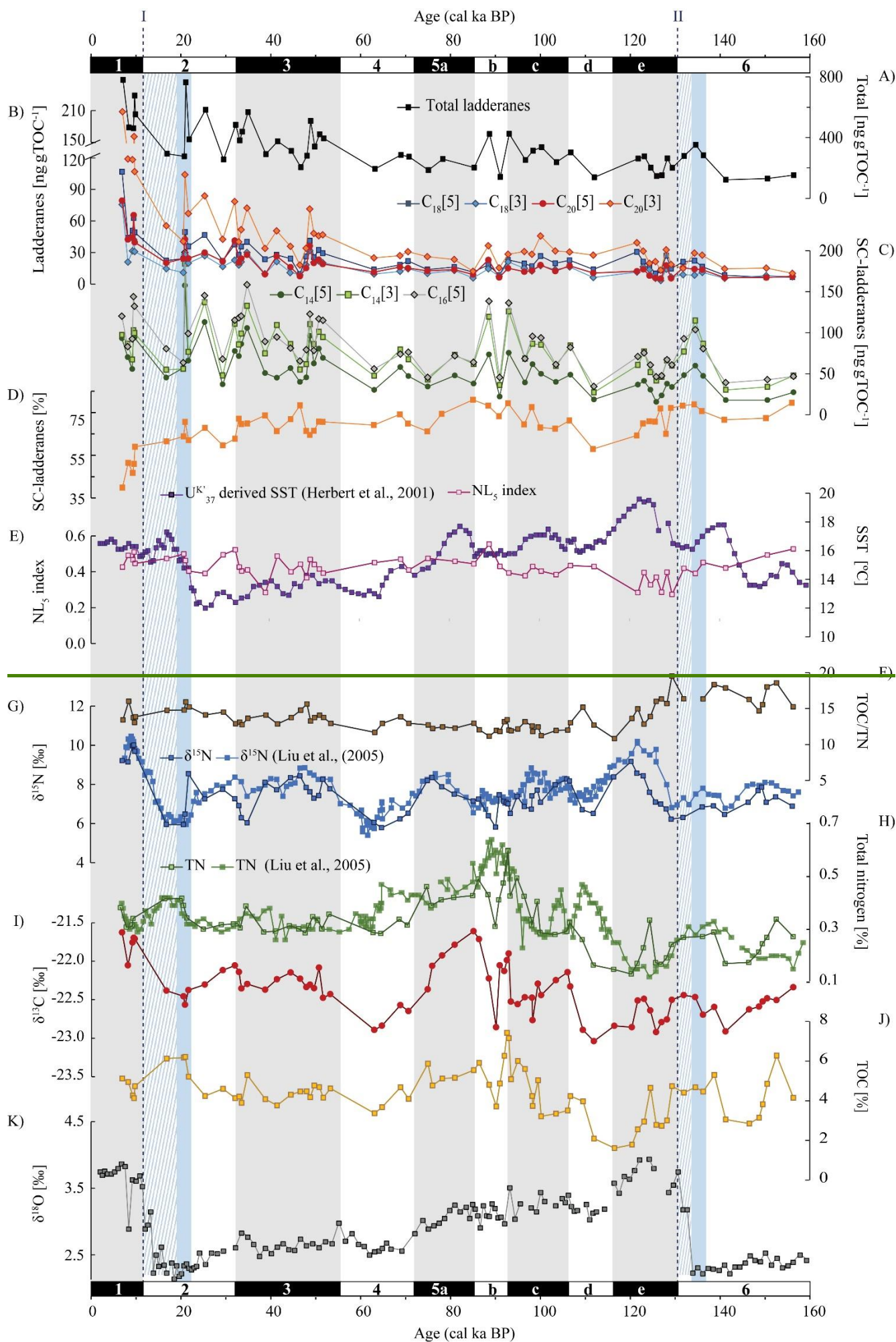
5 Discussion

In the sediment record of ODP site 1012, C₁₈[3]-, C₁₈[5]-, C₂₀[3]- and C₂₀[5]-ladderane FAs and their short chain C₁₄[3]-, C₁₄[5]-, C₁₆[5]-products were detected over the last 500 kyr (~38 mbsf; Fig. 3). This poses a considerable extension of the ladderane record (formerly detected up to ~140 ka BP in Arabian Sea sediments; ~10 mbsf; Jaeschke et al., 2009). Below, we will first discuss the provenance of the detected ladderane lipids (section 5.1). Then, their variability throughout glacial-interglacial cycling (section 5.2), ending with the subsequent implications on our understanding of the nitrogen cycle of the CCS (section 5.3). Unfortunately, the coarse sampling resolution in >160 cal ka BP sediments and low ladderane FA

259 [concentrations \(due to diagenesis\) complicate interpretations of ladderane FA fluctuations in these sediments.](#) Therefore,
260 analysis of trends in ladderane concentrations over (inter)glacial cycling is limited to <160 cal ka BP sediments.

261 **5.1 Ladderanes sourced from anammox bacteria in the ESTNP OMZ water column**

262 The relative contribution of SC-ladderanes to the total ladderane pool is a measure of oxygen exposure (Rush et al., 2011,
263 2012b), and the NL₅-index is a measure of the water temperature of the niche of anammox bacteria (Rattray et al., 2010). In
264 combination, these data may provide insights into the origin of ladderanes in the CCS sediment record.



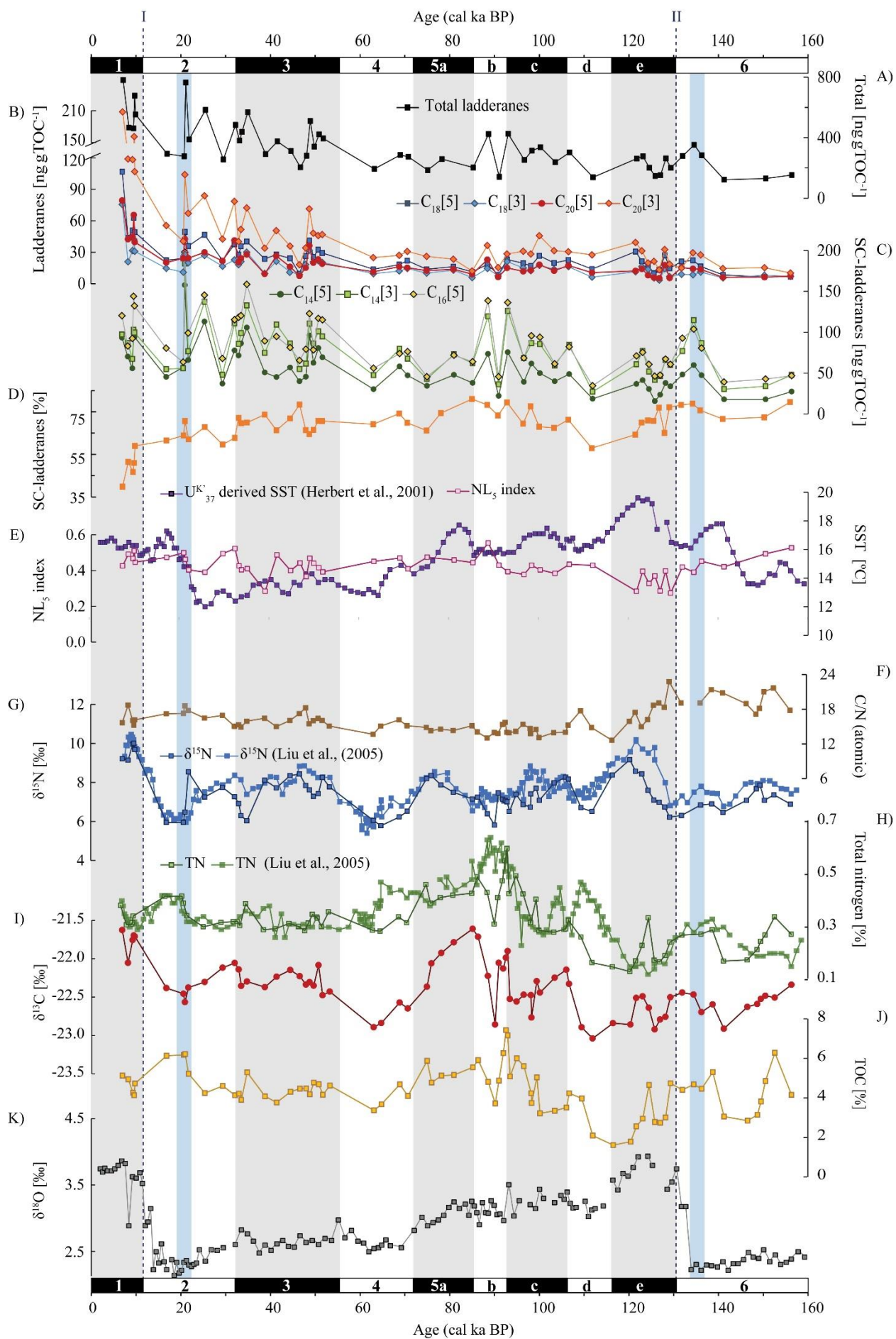


Figure 4: From top to bottom: concentrations of A) total ladderenes (summed SC-ladderanes and ladderanes), B) ladderanes and C) SC-

ladderanes (normalized against TOC [ng gTOC⁻¹]), D) relative abundance of SC-ladderanes over total ladderanes [%], E) U^K₃₇ derived sea-surface temperatures (SST) from Herbert et al., (2001) [°C] and the NL₅-index from this study, F) atomic ratio of total organic carbon (TOC) over total nitrogen (TN), G) bulk sedimentary δ¹⁵N from Liu et al., (2005) and this study [%], H) TN from Liu et al., (2005) and this study [%], I) bulk sedimentary δ¹³C [‰], J) TOC [%] and K) benthic δ¹⁸O record from Herbert et al., (2001) [‰]. All data is derived from the same location (ODP site 1012). Marine isotope stages (MIS) are indicated with black and white bars. Periods of maximum global ice volume (Herbert et al., 2001; blue bars) and the approximate timing of glacial terminations TI and TII (dashed lines) are also indicated.

~~At ODP site 1012, the enriched sedimentary δ¹⁵N signal have been interpreted to derive from the transport of denitrified waters from~~ In the CCS, a progressive depletion of both the water column δ¹⁵N_{NO3} and sedimentary δ¹⁵N signal occurs with increasing latitude, resulting in more depleted values at ODP site 1012 (8–10 ‰; Altabet et al., 1999; Liu et al., 2005; this study) than in the ETNP OMZ core. The northward transport of denitrified waters by the poleward flowing oxygen-poor CU from the core of the ETNP has been evoked to explain this trend. (Castro et al., 2001; Kienast et al., 2002). This means that at ODP site 1012, the sedimentary δ¹⁵N signal is thought to predominantly derive from the ETNP, and not the ESTNP OMZ. In order to understand the observed ladderane trends in the ODP site 1012 record, it is thus important to establish whether the detected ladderanes reflect a local signal (from the ESTNP OMZ) or whether they are also sourced from the ETNP OMZ core and similarly transported northwards with the CU, towards ODP site 1012. Alternatively, ladderanes could also be synthesized by sedimentary anammox bacteria (Vossenberg et al., 2008). ~~However, a similar mechanism is unlikely to explain the presence of ladderane FAs at ODP site 1012. Ladderane FAs are relatively labile compounds, and in the Arabian Sea have been shown to already degrade into their SC products (at relative proportions of ~20 %) within the OMZ water column (DO <3 μmol L⁻¹). There, the sinking of ladderanes through the oxygenated bottom waters underlying the OMZ ultimately resulted in a relative abundance SC ladderanes in the surface sediments of 20–80 %, depending on water column dept.~~

At ODP site 1012, SC-ladderanes were present ~~in similar~~ relative abundances of (40–88 %) throughout the record (Fig. 4D). Ladderane FAs are relatively labile compounds, and in the Arabian Sea have been shown to already degrade into their SC-products (at relative proportions of ~20 %) within the OMZ water column (DO <3 μmol L⁻¹). There, the sinking of ladderanes through the oxygenated bottom waters underlying the OMZ ultimately resulted in similar relative abundances of SC-ladderanes in the surface sediments of 20–80 %, depending on water column depth (Rush et al., 2012b). The similarly high contribution of SC-ladderanes in the ODP 1012 record suggest ladderanes are also sourced from an overlying OMZ water column (i.e. the ESTNP OMZ) and sunk through oxygenated bottom waters before being deposited on the seafloor, which readily became anoxic in view of the high TOC content (Fig. 4J).

298 An OMZ water column source is consistent with [the NL₅ index \(0.3–0.8; Fig. 4Ee derived temperatures \(13–17°C;](#)
299 [S1, Table 6\)](#). According to the NL₅-calibration by Rattray et al., (2010), NL₅ indices within this range more closely reflect
300 [water column rather than sedimentary anammox bacteria. Also, NL₅-derived temperatures, which \(13–17°C; S1, Table 6\) are](#)
301 [are significantly higher than what would be expected for sea-floor temperatures \(i.e., modern annual average bottom water](#)
302 [temperatures at site 1012 are <5°C; WOA, 2018\).](#) Additionally, while the transport of ladderane FAs has been shown to
303 occur within oxygen-depleted systems (van Kemenade et al., 2022), long-distance transport of ladderane FAs with the CU
304 (characteristic DO concentration of ~62 μmol L⁻¹ in modern CU water; Sahu et al., 2022) is unlikely, and would be expected
305 to yield higher relative abundances of SC-ladderane FAs than detected in the record. Transport of ladderanes is also not
306 reflected in present-day ENP ladderane distributions, as an investigation of ladderanes at a more northerly (~20°N) and a
307 more southerly (~17°N) located site showed *in situ* synthesis by pelagic *Ca. Scalindua* at both sites (Sollai et al., 2015).
308 Hence, ladderane FAs are thought to predominantly derive from the ESTNP OMZ water column and reflect a local
309 anammox signal, [although some contribution of allochthonous or sedimentary anammox cannot be entirely excluded.](#)

310 5.2 Anammox variability in the CCS over the last 160 kyr

311 5.2.1 The Holocene and MIS-5, including the penultimate interglacial of MIS 5e

312 Over the ~500 cal ka BP record, ladderane FAs are observed to decrease logarithmically with time (Fig. 3; R² = 0.70), in
313 which the degradation constant *k* follows a linear relationship (when logarithmically transformed; Fig. 5A; R² = 0.88) with
314 time. This is consistent with first order degradation kinetics, typical for OM (Canuel and Martens, 1996). As such, it is not
315 surprising that the highest ladderane concentrations are observed in the youngest sediments, deposited during the early to
316 mid-Holocene. Even so, ladderane FAs normalized against TOC also show elevated concentrations in Holocene sediments.
317 This suggests high ladderane FAs at this time are not simply a preservation signal but also reflect an increase (compared to
318 pre-Holocene sediments) in their production by *Ca. Scalindua* spp. relative to the total organic C pool. Moreover, elevated
319 ladderanes in early to mid-Holocene sediments coincide with enriched bulk δ¹⁵N (9–10 ‰; [Fig. 4G](#)), indicative of enhanced
320 N-loss by anaerobic microorganisms, and elevated TOC and TN concentrations (Fig. 4H, J), indicative of increased
321 productivity.

322 [In contrast to ladderane FAs, concentrations of their SC-products](#) are not highest in Holocene sediments.
323 Consequently, the SC-ladderane data does not fit the logarithmic decrease with time well (R² = 0.4734; [Fig. 3Fig-X](#)), which
324 is also reflected in the relationship of the degradation constant *k* with time (Fig. 5A; R² = 0.43). The oxidation of ladderane
325 FAs to produce SC-ladderane FAs (Rush et al., 2011) has been shown to take place within the oxic waters below the OMZ.
326 In this way, 20–80 % of the ladderane FAs were transformed into SC-ladderanes in the Arabian Sea (Rush et al., 2012c).
327 Throughout the deeper CCS sedimentary record (>10 cal ka BP), the relationship between ladderane FAs and their SC-

328 products follows a linear trend ($R^2 = 0.878$; Fig. 5B), with SC-ladderanes making ~60–80 % of total ladderanes (Fig. 4D).
329 However, in Holocene sediments (<10 cal ka BP sediments), the relationship between ladderanes and SC-ladderanes is
330 different (Fig. 5B), and SC-ladderanes occur at relatively lower abundance (40– 60 % ~~in Fig. 4~~) compared to the rest of the
331 record. This indicates that after 10 cal ka BP, there was no significant change in the exposure of ladderane FAs to the
332 oxygenated water underlying the ETNP OMZ before being buried in the sediment record, but that in the recent record, there
333 was reduced oxygen exposure.

334 Reduced oxygen exposure is likely to have resulted from an intensified OMZ; Lembke-Jene et al. (2018) showed,
335 using palaeoceanographic proxies and palaeomodeling, that a combination of sea ice loss, increased SST and
336 remineralization rates led to more deoxygenated intermediate waters (the NPIW) during the early to mid-Holocene in the
337 North Pacific. Moreover, in the ETNP, enriched sedimentary $\delta^{15}\text{N}$ values and laminated sediments during the early
338 Holocene, alongside geochemical tracers, have been interpreted to signal the presence of a strong OMZ at this time, while
339 bioturbated sediments occurred over the last glacial period (Thunell and Kepple, 2004).

340 Ladderane FAs concentrations also peak during the penultimate interglacial (the Eemian; MIS 5e), in line with
341 enriched (>8 ‰) $\delta^{15}\text{N}$ values. Microfossil data from MIS 5 has indicated that intermediate waters in the western North
342 Pacific were more deoxygenated during the Eemian (Matul et al., 2016), which may have driven increased anammox in the
343 CCS at this time. Yet, while $\delta^{15}\text{N}$ values over MIS 5 maximize during MIS 5e, ladderane FAs concentrations peak during
344 mid-MIS 5 (MIS 5b–c; Fig. 4). During MIS 5b–d, when (SC-)ladderane FA concentrations maximize, intermediate waters in
345 the western North Pacific were likely oxic (Matul et al., 2016) and the $\delta^{15}\text{N}$ signal is more subdued (<8 ‰; Fig. 4Gg). At
346 this time, increased (SC-)ladderane FAs coincide with ~~Nonetheless, peaks in~~ paleo-productivity proxies (i.e., TOC and TN);
347 also peak during MIS 5b–c (Fig. 4H, Jh–j). Remineralization of increased phytoplankton biomass may consequently have led
348 to more reduced local conditions, favouring anammox. ~~Indeed, o~~ Over the course of MIS 5, from late MIS 5e onwards,
349 SSTs in the CCS decreased while the CC strengthened (Herbert et al., 2001; Yamamoto et al., 2007). This would have led to
350 increased transport of high-oxygen, nutrient-rich NPIW (Herguera et al., 2010) and enhanced open ocean upwelling. This
351 ~~would~~ may have fuelled productivity, as reflected in which explains the high TOC and TN concentrations in mid-MIS 5.

352 The C/N ratio remains fairly stable throughout MIS 1 to MIS 5c (MN = 16, STD = 2); Fig. 4F), with higher values
353 observed during MIS 6 (MN = 20, STD = 2; discussed in section 5.2.2). Based on stoichiometry, enhanced NO_3^- supply is
354 expected to lower the ratio in phytoplankton biomass (Matsumoto et al., 2020). Yet, changes in nutrient concentrations have
355 been observed to effect the C/P and N/P, but not the C/N ratio (Frigstad et al., 2011). It is therefore not surprising that the
356 increased TN content during mid-MIS 5 is not reflected in the C/N ratio. Also, while the $\delta^{13}\text{C}$ signal (-23 to -22 ‰; Fig. 4I)
357 reflects a typical marine origin of OM, the C/N ratio is higher than commonly observed for marine algae (e.g., Lamb et al.,

2006). [This is likely caused by preferential remineralization of organic N during the settling of OM from the photic zone](#) (Verardo & McIntyre, 1994; Schneider et al., 2003).

During mid-MIS 5, [where TN and TOC peak](#), anammox may have been fuelled by local increases in OM-supply. Babbitt et al., (2014) showed, using incubations from the ETNP OMZ, that anammox rates increase in response to the addition of OM. Likewise, in the modern Southern Pacific OMZ, N-loss by anammox was found to be strongly correlated with the export of OM, via the release of ammonium into the water column through remineralization (Kalvelage et al., 2013). [As such, the co-occurrence of ladderane FA and paleo-productivity proxies maxima during MIS 5](#), could reflect an increase in *Ca. Scalindua* spp. abundance in response to an increased N-substrate supply via OM-remineralization or nutrient transport. [Remineralization of increased phytoplankton biomass may consequently also have led to more reduced local conditions, which would also favour anammox. This local signal would not have been recorded in the western part of the North Pacific, where intermediate waters were oxic](#) (Matul et al., 2016). [The relatively subdued \$\delta^{15}\text{N}\$ signal during mid-MIS 5](#), and consequent implications for our understanding of the N-cycle in the CCS are further discussed in section 5.3. [Yet, this is only expected if phytoplankton is predominantly eukaryotic. A dominant cyanobacterial](#)

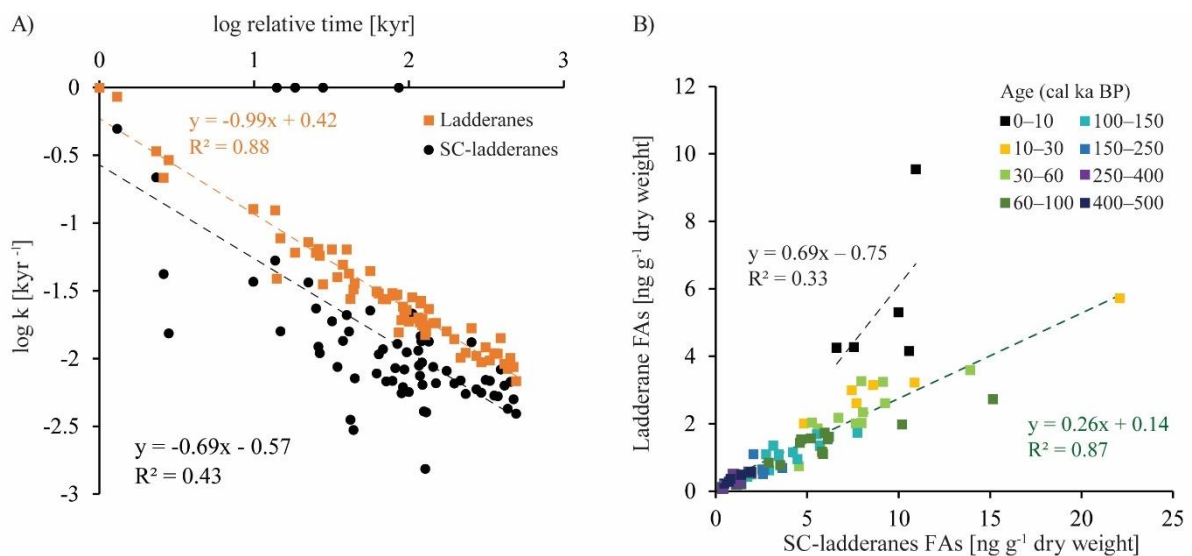


Figure 5: A) Linear relationship between the logarithmic values of the degradation constant k and relative time for ladderane FAs (orange squares) and SC-ladderane FAs (black dots). B) Relationship between ladderane FAs and SC-ladderane FAs, in which samples are colour-coded according to age. The linear relationship and corresponding R^2 are given for the most recent age group (0-10 cal ka BP; in black) and the >10 cal ka BP age groups (in green).

5.2.2 The two most recent glacial periods

Ladderane FAs are observed to increase from early MIS 3 to mid-MIS 2, and from mid- to late-MIS 6. Maxima of ladderanes occur approximately at the timing of icesheet volume maxima of the last glacial maxima (LGM) and the penultimate glacial of MIS 6 (blue bars in Fig. 4; following timing of Herbert et al., 2001). During the last glacial period

380 (~115–12 ka BP) and the penultimate glacial MIS 6, large parts of the North American continent were covered by the
381 Laurentide and Cordilleran ice sheets. While glacials are typically associated with a well-ventilated intermediate-water mass
382 (Herguera et al., 2010) and a strong southward advection of the CC (Ortiz et al., 1997), a weakening of the CC has been
383 proposed to occur at times of global ice sheet maxima. In the CCS, $U_{37}^{K'}$ -derived temperatures indicate that SSTs increased
384 ~12 kyr in advance of maximal ice-sheet volumes. This is thought to reflect increased northward advection of warm oxygen-
385 poor waters carried by the CU and DC in response to a weakened CC due to large ice-sheet volumes (Herbert et al., 2001).
386 Using trace elements, Cartapanis et al., (2011) found that intermediate water oxygenation off Baja California deteriorated
387 slightly over the course of late MIS 3 and early MIS 2, consistent with a strengthening of the CU at this time. As such, the
388 increased abundance of ladderanes observed during (and leading up to) ice sheet maxima at ODP site 1012, may derive from
389 an increased *Ca. Scalindua* spp. abundance due to more reduced local conditions, via the enhanced strength of the CU.

390

391 MIS 6 and its termination (T2) are further characterized by relatively high C/N ratios (17–23; Fig. 4F). Matsumoto
392 et al., (2020) found, using a global ocean carbon cycle model, that during glacial periods the expansion of sea ice increased
393 global C:N:P ratios. Additionally, taxonomic changes during glacials, in which eukaryotic phytoplankton became more
394 dominant, resulted in NO_3^- depletion (hereby increasing the C/N ratio). At the same time, decreased upwelling during glacial
395 periods in the North Pacific (Worne et al., 2019) may have also lowered nutrient availability. Low N-availability is reflected
396 in relatively low TN concentrations in this record (Fig. 4H). This suggests anammox at this time was primarily promoted by
397 reduced local DO concentrations via enhanced CU strength, rather than enhanced nutrient supply and/or increased
398 remineralization rates.

399 While enhanced anammox in response to deoxygenation during glacial maxima is at odds with previous
400 assessments of N-loss in the CCS (e.g., Liu et al., 2005), deoxygenation of the Pacific is consistent with recent paleo-proxy
401 studies (Lu et al., 2016; Anderson et al., 2019) and modelling results (Matsumoto et al., 2020). According to these studies,
402 many parts of the glacial ocean, including the equatorial Pacific, had substantially lower DO during the last glacial period
403 than today. This fits with increased ladderane FAs at this time, which suggests N-loss in the CCS was likely more intense
404 during glacial maxima than previously assumed.

405 ~~In contrast, low ladderane concentrations occur at times of deglaciation (T1: ~19–11 ka BP and T2: ~135–128 ka BP).~~
406 ~~Modelling studies have proposed that during the early part of the Last Glacial Termination (~17.5–15.0 ka BP), a~~
407 ~~reorganization of the global conveyor belt circulation would have led to deep water formation in the North Pacific, extending~~
408 ~~to ~2500 to 3000 mbss. In turn, this would have led to nutrient poor but well-ventilated intermediate deep~~
409 **5.3 Implications**
of the occurrence of anammox on the N cycle in the CCS

410 In the CCS, previous estimates of changes in N-loss over time have been based on the bulk sedimentary $\delta^{15}\text{N}$ record.
411 Enriched $\delta^{15}\text{N}$ during interglacials (7–10 %) are thought to reflect intensified denitrification in response to reduced DO,
412 while more depleted $\delta^{15}\text{N}$ during glacials (4–6 %) are assumed to reflect lowered rates in response to increased DO (Liu et
413 al., 2005; 2008). ~~However, the occurrence of ladderane FAs throughout our CCS record~~ ~~However, the high abundance of~~
414 ~~ladderane FAs throughout our CCS record (i.e. up to a factor ~5 higher than in the Arabian Sea record)~~ now shows that
415 anammox was (also) responsible for N-loss and thus contributed, at least partially, to the sedimentary $\delta^{15}\text{N}$ record.

416 The cross-correlation for both $\delta^{15}\text{N}$ – $\delta^{18}\text{O}$ and $\delta^{18}\text{O}$ –SST at ODP site 1012 (Liu et al., 2005) indicates that
417 fluctuations in $\delta^{15}\text{N}$ occur in tandem with glacial-interglacial cycling. However, a long-standing conundrum has been the
418 discrepancy between the $\delta^{15}\text{N}$ record and productivity proxies (i.e., TOC and TN), especially north of the ETNP (Kienast et
419 al., 2002), as also seen in our record (Fig. 4). This decoupling has been used previously to suggest that variations in
420 denitrification was not due to changes in OM remineralization rate, but rather from changes in ocean circulation and
421 ventilation patterns (Ganeshram et al., 2000). Yet, fluctuations in ladderanes *do* seem to follow trends in paleo-productivity
422 proxies (i.e., TOC and TN) relatively closely, especially during the Holocene, MIS 3 and MIS 5. And, while enriched $\delta^{15}\text{N}$
423 values sometimes correspond to ladderane maxima (i.e. during the Holocene), discrepancies with ladderane concentrations
424 are seen especially during ~~MIS 3 and~~ MIS 5, and during glacial periods (Fig. 4).

425 This may suggest that increased anammox does not always correspond to increased N-loss, possibly via
426 simultaneously reduced denitrification rates (Koeve and Kähler, 2010). Yet, Babbin et al., (2014) showed, using incubations
427 from the ETNP OMZ, that both denitrification and anammox are limited by OM supply, and their rates increase in response
428 to the addition of OM. Moreover, these authors showed that both denitrifiers and anammox bacteria are similarly inhibited
429 by oxygen in the marine environment, at DO concentration above-around 3 to 8 $\mu\text{mol L}^{-1}$ (Babbin et al., 2014). ~~Furthermore,~~
430 ~~Babbin et al., (2014) showed, using incubations from the ETNP OMZ, that both denitrification and anammox are limited by~~
431 ~~OM supply, and their rates increase in response to the addition of OM.~~ ~~As anammox bacteria are autotrophic, this may be~~
432 ~~explained by the dependence of the process on NH_4^+ and NO_2^- availability, which can a.o. be supplied via remineralization.~~
433 As such, both anammox and denitrification should respond similarly to changes in DO and OM in the CCS.

434 Moreover, gi~~Out of phase anammox and denitrification could be caused by variations in the C/N ratio of OM.~~
435 ~~Given~~ the average C/N signature of marine OM (106:16; Redfield, 1963), stoichiometric constraints should result in a ratio
436 of N_2 production via denitrification and anammox of 71:29 (Koeve and Kähler, 2010)~~9~~. On the one hand, this means that the
437 relative contribution of anammox to N_2 -production is likely lower than the contribution of denitrification, possibly resulting
438 in a less strong influence of anammox on the $\delta^{15}\text{N}$ signal. On the other hand, this means that denitrification and anammox
439 rates should be positively related, in which increased anammox is associated with increased denitrification (Koeve and
440 Kähler, 2010). Potentially, anammox and denitrification could be unsynchronized (as indicated by differences between the

441 ladderane and $\delta^{15}\text{N}$ records) in response to variations in the C/N ratio of OM. Localized variations in the C/N signature may
442 result in different relative contributions. Yet, integrating these variations over space and time should obtain a similar ratio
443 (Dalsgaard et al., 2012; Babbin et al., 2014; Ward, 2013). Additionally, the C/N ratio remains fairly consistent throughout
444 the record (13–19), except during MIS 6 where it is higher (17–23; Fig. 4F) and variations do not correspond to those
445 observed in ladderane FAs or $\delta^{15}\text{N}$. As such, given the temporal resolution of the record (which does not cover seasonality),
446 denitrification and anammox intensities are expected to fluctuate in-tandem.

447 Consequently, variability in $\delta^{15}\text{N}$ of the CCS sedimentary record may, at times, simply not relate directly to changes
448 in denitrification and/or anammox rates. Reconstructions of N-loss using sedimentary $\delta^{15}\text{N}$ depend on the assumption that
449 there was complete biological utilization of NO_3^- by phytoplankton. However, during periods of high upwelling intensity (as
450 likely occurred during mid-MIS 5; see section 5.2.1), the high NO_3^- availability may result in incomplete NO_3^- assimilation.
451 This allows for the preferential uptake of ^{14}N by primary producers, resulting in a pool of $\delta^{15}\text{N}$ depleted OM available for
452 heterotrophic denitrification (Tesdal et al., 2013). Hence, at times of high NO_3^- supply, incomplete nitrate assimilation
453 would have quenched the $\delta^{15}\text{N}$ signal, even if denitrification was as intense as during periods of low NO_3^- availability.
454 Moreover, a study by Altabet and Francois (1994) showed that sedimentary $\delta^{15}\text{N}$ in the equatorial Pacific records the
455 isotopic enrichment of near-surface NO_3^- via depletion by phytoplankton, in which enriched $\delta^{15}\text{N}$ values are associated with
456 reduced NO_3^- availability for phytoplankton assimilation. Also, in the South Pacific, NO_3^- concentrations have been found to
457 affect the $U^{K'}_{37}$ index (Placencia et al., 2010). Given the phase-relationship between the $\delta^{15}\text{N}$ and $U^{K'}_{37}$ -based SST records
458 of the CCS (Liu et al., 2008) and the discrepancies between the $\delta^{15}\text{N}$ and ladderane records, it may be reasonable to conclude
459 that the CCS sedimentary $\delta^{15}\text{N}$ fluctuations (also) record variations in NO_3^- assimilation by phytoplankton.

460 Additionally, other biological processes may influence the $\delta^{15}\text{N}$ signal (Zonneveld et al., 2010). In the Gulf of
461 Tehuantepec, at the southern end of the ETNP OMZ core, $\delta^{15}\text{N}$ values decrease over the course of the Holocene (Thunell and
462 Kepple, 2004; Hendy and Pedersen, 2006), while laminated sediments suggest reduced DO concentrations. This was
463 interpreted as being the result of increased N_2 -fixation ($\epsilon: \leq +2\text{‰}$; Sigman and Fripiat, 2019), which lowered the
464 “denitrification” $\delta^{15}\text{N}$ signal (Thunell and Kepple, 2004). Lastly, enrichment of the sedimentary $\delta^{15}\text{N}$ values occurs during
465 early burial, where oxygen exposure results in enhanced biological isotopic alteration (Robinson et al., 2012). In short,
466 sedimentary $\delta^{15}\text{N}$ is shaped by many opposing processes, and assuming a one-on-one relationship with denitrification
467 intensities and DO concentration clearly misses the complexity that shape the CC system. Ladderanes hereby offer a more
468 detailed picture of N-loss dynamics in the paleoenvironment of the CCS. In the case of the ODP site 1012 record, ladderane
469 concentration trends challenge the conventional assumption that N-loss processes solely follow ocean circulation and
470 ventilation patterns coupled to (inter)glacial cycling, and instead show OM remineralization may also be an important driver
471 of N-loss.

472 Discrepancies between the ladderane and $\delta^{15}\text{N}$ -record hereby necessitate careful consideration when applying N-
473 isotope based budgets to estimate past N-cycling. More specifically, the occurrence of increased ladderane concentrations
474 during glacial maxima may require a re-evaluation on the response of N-loss rates to glacial-interglacial cycling in the CCS.
475 Furthermore, the occurrence of an additional N-loss pathway in the CCS (anammox), other than denitrification, may affect
476 estimates of N_2O greenhouse-gas production by denitrifiers and the degree of heterotrophy of the system, although the
477 importance of this would require further investigation. Future research, investigating anammox biomarkers in other CCS
478 records (preferably in a latitudinal gradient with this record) may offer further insights into N-loss dynamics across glacial-
479 interglacial cycles.

480 **6 Conclusion**

481 Ladderane FAs detected in a ~500 kyr CCS sedimentary record at ODP site 1012 reveal the past occurrence of anaerobic
482 ammonium oxidising (anammox) bacteria in the water column of the California current system (CCS) over the last five
483 glacial terminations. The index of ladderanes with five cyclobutene moieties (NL_5), which correlates with the *in situ*
484 temperature at which ladderanes are synthesised, suggests that ladderanes were derived from the ETSNP OMZ water
485 column. [The CCS record shows](#) a continuous presence of ladderane FAs over the last two interglacial-glacial transitions,
486 with maxima during: i) the Holocene, ii) leading up to and during the LGM (early MIS 3 to mid-MIS 2), iii) MIS 5b-c and
487 iv) during the ice sheet maxima of the penultimate glacial (late MIS 6). Combining information on the presence of
488 ladderanes with paleo-productivity proxies and the hydrographic features of the CCS suggests anammox abundance was
489 driven both by OM-remineralization and advection changes, which regulated nutrient and oxygen concentrations. In the
490 record, a clear shift is seen in the relationship of SC-ladderanes over their parent products, in which the relative abundance of
491 SC-ladderanes is significantly lower in Holocene than in pre-Holocene sediments. This may reflect a shift in oxygen
492 exposure, which corresponds to previous studies showcasing a vertical expansion of the ENP OMZ over the Holocene.
493 Clearly, the anammox contribution to N-loss in the CCS, as shown in this study, requires a reassessment of biogeochemical
494 cycling in this system. Discrepancies between the ladderane and $\delta^{15}\text{N}$ record may imply that N-loss was perhaps more
495 intense during cold phases than previously assumed. Careful considerations must thus be taken when using N-isotope based
496 budgets to estimate past N-cycling in the CCS; sedimentary $\delta^{15}\text{N}$ is shaped by many opposing processes, and assuming a
497 one-to-one relationship between N-loss intensities and OMZ variability clearly overlooks the complexity that shapes the CC
498 system. Ladderanes hereby offer a more holistic picture of N-loss dynamics in the paleoenvironment of the CCS.

499 **Data availability.** All data discussed in this paper is available in the supplementary material 1. Data from supplementary
500 material 1 can be retrieved via the following doi: [10.25850/nioz/7b.b.sg](https://doi.org/10.25850/nioz/7b.b.sg)

501 **Supplement.** The supplement related to this article is available on-line at:

502 **Author contributions.** ZE and ZRvK performed the laboratory work. ZRvK conducted the data analysis and writing of the
503 manuscript. ZE created the age-model. ECH developed and optimized the UHPLC-HRMS method for the analysis of
504 ladderane lipids. DR provided the supervision of the project. DR, ZE and ZRvK designed and conceptualized the project.
505 JSSD provided critical support in data interpretation. All authors contributed to the writing of the manuscript.

506 **Competing interests.** The authors declare that they have no conflict of interest.

507 **Acknowledgements.** We thank the captain and crew of Ocean Drilling Program Leg 167 for the collection of all sampled
508 material used in this study. Denise Dorhout and Monique Verweij are also greatly appreciated for their support with the
509 instrumental analysis. We also kindly thank Ronald van Bommel and Marcel van der Meer for their help in the isotope lab.

510 **Financial support.** This research was supported by the Soehngen Institute of Anaerobic Microbiology (SIAM) Gravitation
511 Grant (024.002.002), awarded to JSSD by the Dutch Ministry of Education, Culture and Science (OCW).

512 **References.**

513 Altabet, M. A. and Francois, R.: Sedimentary nitrogen isotopic ratio as a recorder for surface ocean nitrate utilization, *Global*
514 *Biogeochem Cycles*, 8, 103–116, <https://doi.org/10.1029/93GB03396>, 1994.

515 Altabet, M. A., Pilskaln, C., Thunell, R., Pride, C., Sigman, D., Chavez, F., and Francois, R.: The nitrogen isotope
516 biogeochemistry of sinking particles from the margin of the eastern North Pacific, *Deep Sea Res 1 Oceanogr Res Pap*, 46,
517 655–679, [https://doi.org/10.1016/S0967-0637\(98\)00084-3](https://doi.org/10.1016/S0967-0637(98)00084-3), 1999.

518 Anderson, R. F., Sachs, J. P., Fleisher, M. Q., Allen, K. A., Yu, J., Koutavas, A., and Jaccard, S. L.: Deep-Sea Oxygen
519 Depletion and Ocean Carbon Sequestration During the Last Ice Age, *Global Biogeochem Cycles*, 33, 301–317,
520 <https://doi.org/https://doi.org/10.1029/>, 2019.

521 Babbin, A. R., Babbin, A. R., Keil, R. G., Devol, A. H., and Ward, B. B.: Oxygen Control Nitrogen Loss in the Ocean, 406,
522 <https://doi.org/10.1126/science.1248364>, 2014.

523 Bakun, A. and Nelson, C. S.: The seasonal cycle of wind-stress curl in subtropical eastern boundary current regions, *J.*
524 *Physical Oceanography*, 21, 1815–1834, [https://doi.org/10.1175/1520-0485\(1991\)021<1815:TSCOWS>2.0.CO;2](https://doi.org/10.1175/1520-0485(1991)021<1815:TSCOWS>2.0.CO;2), 1991.

525 Bograd, S. J., Castro, C. G., di Lorenzo, E., Palacios, D. M., Bailey, H., Gilly, W., and Chavez, F. P.: Oxygen declines and
526 the shoaling of the hypoxic boundary in the California Current, *Geophys Res Lett*, 35, 1–6,
527 <https://doi.org/10.1029/2008GL034185>, 2008.

528 Bograd, S. J., Schroeder, I., Sarkar, N., Qiu, X., Sydeman, W. J., and Schwing, F. B.: Phenology of coastal upwelling in the
529 California Current, *Geophys Res Lett*, 36, 1–5, <https://doi.org/10.1029/2008GL035933>, 2009.

530 Brunner, B., Contreras, S., Lehmann, M. F., Matantseva, O., Rollog, M., and Kalvelage, T.: Nitrogen isotope effects induced
531 by anammox bacteria, 2–7, <https://doi.org/10.1073/pnas.1310488110>, 2013.

532 Canuel, E. A. and Martens, C. S.: Reactivity of recently deposited organic matter : near the sediment-water Degradation
533 interface of lipid compounds, 60, 1793–1806, 1996.

534 Cartapanis, O., Tachikawa, K., and Bard, E.: Northeastern Pacific oxygen minimum zone variability over the past 70 kyr :
535 Impact of biological production and oceanic ventilation, 26, 1–17, <https://doi.org/10.1029/2011PA002126>, 2011.

536 Castro, C. G., Chavez, F. P., and Collins, C. A.: Role of the California undercurrent in the export of denitrified waters from
537 the eastern tropical North Pacific, *Global Biogeochem Cycles*, 15, 819–830, <https://doi.org/10.1029/2000GB001324>, 2001.

538 Chavez, F. P. and Messié, M.: A comparison of Eastern Boundary Upwelling Ecosystems, *Prog Oceanogr*, 83, 80–96,
539 <https://doi.org/10.1016/j.pocean.2009.07.032>, 2009.

540 Checkley, D. M. and Barth, J. A.: Patterns and processes in the California Current System, *Prog Oceanogr*, 83, 49–64,
541 <https://doi.org/10.1016/j.pocean.2009.07.028>, 2009.

542 Choumiline, K., Pérez-Cruz, L., Gray, A. B., Bates, S. M., and Lyons, T. W.: Scenarios of Deoxygenation of the Eastern
543 Tropical North Pacific During the Past Millennium as a Window Into the Future of Oxygen Minimum Zones, *Front Earth Sci*
544 (Lausanne), 7, 1–23, <https://doi.org/10.3389/feart.2019.00237>, 2019.

545 Codispoti, L. A., Brandes, J. A., Christensen, J. P., Devol, A. H., Naqvi, S. W. A., Paerl, H. W., and Yoshinari, T.: The
546 oceanic fixed nitrogen and nitrous oxide budgets: Moving targets as we enter the anthropocene?, *Sci Mar*, 65, 85–105,
547 <https://doi.org/10.3989/scimar.2001.65s285>, 2001.

548 Dalsgaard, T., Thamdrup, B., Farías, L., and Revsbech, N. P.: Anammox and denitrification in the oxygen minimum zone of
549 the eastern South Pacific, *Limnol Oceanogr*, 57, 1331–1346, <https://doi.org/10.4319/lo.2012.57.5.1331>, 2012.

550 Dorman, C. E. and Winanat, C. D.: Buoy observations of the atmosphere along the west coast of the United States, 1981–
551 1990, *J Geophys Res*, 100, 1981–1990, <https://doi.org/10.1029/95jc00964>, 1995.

552 Fine, R. A., Maillet, K. A., Sullivan, K. F., and Willey, D.: Circulation and Ventilation flux of the Pacific Ocean, *J Geophys*
553 *Res Oceans*, 106, 22159–22178, <https://doi.org/10.1029/1999jc000184>, 2001.

554 Frigstad, H., Andersen, T., Hessen, D. O., Naustvoll, L. J., Johnsen, T. M., and Bellerby, R. G. J.: Seasonal variation in
555 marine C:N:P stoichiometry: Can the composition of seston explain stable Redfield ratios?, *Biogeosciences*, 8, 2917–2933,
556 <https://doi.org/10.5194/bg-8-2917-2011>, 2011.

557 Fu, W., Bardin, A., and Primeau, F.: Tracing ventilation source of tropical pacific oxygen minimum zones with an adjoint
558 global ocean transport model, *Deep Sea Res 1 Oceanogr Res Pap*, 139, 95–103, <https://doi.org/10.1016/j.dsr.2018.07.017>,
559 2018.

560 Galán, A., Molina, V., Thamdrup, B., Woebken, D., Lavik, G., Kuypers, M. M. M., and Ulloa, O.: Anammox bacteria and
561 the anaerobic oxidation of ammonium in the oxygen minimum zone off northern Chile, *Deep Sea Res 2 Top Stud Oceanogr*,
562 56, 1021–1031, <https://doi.org/10.1016/j.dsr2.2008.09.016>, 2009.

563 Ganeshram, R. S., Pedersen, T. F., Calvert, S. E., McNeill, G. W., and Fontugne, M. R.: Glacial-interglacial variability in
564 denitrification in the World ' s Oceans : Causes and consequences, *Paleoceanography*, 15, 361–367, 2000.

565 van de Graaf, A. A., Mulder, A., de Bruijn, P., Jetten, M. S. M., Robertson, L. A., and Kuenen, J. G.: Anaerobic oxidation of
566 ammonium is a biologically mediated process, *Appl Environ Microbiol*, 61, 1246–1251,
567 <https://doi.org/10.1128/aem.61.4.1246-1251.1995>, 1995.

568 van de Graaf, A. A., de Bruijn, P., Robertson, L. A., Jetten, M. S. M., and Kuenen, J. G.: Metabolic pathway of anaerobic
569 ammonium oxidation on the basis of 15N studies in a fluidized bed reactor, *Microbiology (N Y)*, 143, 2415–2421,
570 <https://doi.org/10.1099/00221287-143-7-2415>, 1997.

571 Gruber, N.: The Ocean Carbon Cycle and Climate, in: *The Ocean Carbon Cycle and Climate*, edited by: Follows, M. and
572 Oguz, T., Dordrecht, <https://doi.org/10.1007/978-1-4020-2087-2>, 2004.

573 Hamasaki, K., Shishikura, R., Suzuki, S., Shiozaki, T., Ogawa, H., Nakamura, T., and Suwa, Y.: Distribution and phylogeny
574 of anaerobic ammonium-oxidizing (anammox) bacteria in the water column of the central Pacific Ocean, *Deep Sea Res 2*
575 *Top Stud Oceanogr*, 156, 60–67, <https://doi.org/10.1016/j.dsr2.2017.11.013>, 2018.

576 Hamersley, M. R., Lavik, G., Woebken, D., Rattray, J. E., Lam, P., Hopmans, E. C., Sinninghe Damsté, J. S., Krüger, S.,
577 Graco, M., Gutiérrez, D., and Kuypers, M. M. M.: Anaerobic ammonium oxidation in the Peruvian oxygen minimum zone,
578 *Limnol Oceanogr*, 52, 923–933, <https://doi.org/10.4319/lo.2007.52.3.0923>, 2007.

579 Hendy, I. L. and Kennett, J. P.: Tropical forcing of North Pacific intermediate water distribution during Late Quaternary
580 rapid climate change?, *Quat Sci Rev*, 22, 673–689, [https://doi.org/10.1016/S0277-3791\(02\)00186-5](https://doi.org/10.1016/S0277-3791(02)00186-5), 2003.

581 Hendy, I. L. and Pedersen, T. F.: Oxygen minimum zone expansion in the Eastern Tropical North Pacific during
582 deglaciation, *Geophys Res Lett*, 33, 1–5, <https://doi.org/10.1029/2006GL025975>, 2006.

583 Herbert, T. D., Schuffert, J. D., Andreasen, D., Heusser, L., Lyle, M., Mix, A., Ravelo, A. C., Stott, L. D., and Herguera, J.
584 C.: Collapse of the California current during glacial maxima linked to climate change on land, *Science* (1979), 293, 71–76,
585 <https://doi.org/10.1126/science.1059209>, 2001.

586 Herguera, J. C., Herbert, T., Kashgarian, M., and Charles, C.: Intermediate and deep water mass distribution in the Pacific
587 during the Last Glacial Maximum inferred from oxygen and carbon stable isotopes, *Quat Sci Rev*, 29, 1228–1245,
588 <https://doi.org/10.1016/j.quascirev.2010.02.009>, 2010.

589 Hopmans, E. C., Kienhuis, M. V. V., Rattray, J. E., Jaeschke, A., Schouten, S., and Sinninghe Damsté, J. S.: Improved
590 analysis of ladderane lipids in biomass and sediments using high-performance liquid chromatography/atmospheric pressure
591 chemical ionization tandem mass spectrometry, *Rapid Communications in Mass Spectrometry*, 20, 2099–2103,
592 <https://doi.org/10.1002/rcm>, 2006.

593 Huyer, A.: Coastal upwelling in the California current system, *Prog Oceanogr*, 12, 259–284, <https://doi.org/10.1016/0079->
594 [6611\(83\)90010-1](https://doi.org/10.1016/0079-6611(83)90010-1), 1983.

595 Jaeschke, A., Ziegler, M., Hopmans, E. C., Reichart, G. J., Lourens, L. J., and Schouten, S.: Molecular fossil evidence for
596 anaerobic ammonium oxidation in the Arabian Sea over the last glacial cycle, *Paleoceanography*, 24,
597 <https://doi.org/10.1029/2008PA001712>, 2009.

598 Kalvelage, T., Lavik, G., Lam, P., Contreras, S., Arteaga, L., Löscher, C. R., Oeschlies, A., Paulmier, A., Stramma, L., and
599 Kuypers, M. M. M.: Nitrogen cycling driven by organic matter export in the South Pacific oxygen minimum zone, *Nat*
600 *Geosci*, 6, 228–234, <https://doi.org/10.1038/ngeo1739>, 2013.

601 Van Kemenade, Z. R., Villanueva, L., Hopmans, E. C., Kraal, P., Witte, H. J., Sinninghe Damsté, J. S., and Rush, D.:
602 Bacteriohopanetetrol-x: Constraining its application as a lipid biomarker for marine anammox using the water column
603 oxygen gradient of the Benguela upwelling system, *Biogeosciences*, 19, 201–221, <https://doi.org/10.5194/bg-19-201-2022>,
604 2022.

605 van Kemenade, Z. R., Cutmore, A., Hennekam, R., Hopmans, E. C., van der Meer, M. T. J., Mojtahid, M., Jorissen, F. J.,
606 Bale, N. J., Reichart, G. J., Sinninghe Damsté, J. S., and Rush, D.: Marine nitrogen cycling dynamics under altering redox
607 conditions: Insights from deposition of sapropels S1 and the ambiguous S2 in the Eastern Mediterranean Sea, *Geochim*
608 *Cosmochim Acta*, 354, 197–210, <https://doi.org/10.1016/j.gca.2023.06.018>, 2023.

609 Kemp, A. E. S., Langhorne, D. N., Fairchild, I. J., Schmitt, T. S., and Nisbet, E. G.: Evidence for abrupt climate changes in
610 annually laminated marine sediments, *Philosophical Transactions of the Royal Society A: Mathematical, Physical and*
611 *Engineering Sciences*, 361, 1851–1870, <https://doi.org/10.1098/rsta.2003.1247>, 2003.

612 Kienast, S. S., Calvert, S. E., and Pedersen, T. F.: Nitrogen isotope and productivity variations along the northeast Pacific
613 margin over the last 120 kyr: Surface and subsurface paleoceanography, *Paleoceanography*, 17, 7-1-7–17,
614 <https://doi.org/10.1029/2001PA000650>, 2002.

615 Kobayashi, K., Makabe, A., Yano, M., Oshiki, M., Kindaichi, T., Casciotti, K. L., and Okabe, S.: Dual nitrogen and oxygen
616 isotope fractionation during anaerobic ammonium oxidation by anammox bacteria, *ISME Journal*, 13, 2426–2436,
617 <https://doi.org/10.1038/s41396-019-0440-x>, 2019.

618 Koeve, W. and Kähler, P.: Heterotrophic denitrification vs. autotrophic anammox-quantifying collateral effects on the
619 oceanic carbon cycle, *Biogeosciences*, 7, 2327–2337, <https://doi.org/10.5194/bg-7-2327-2010>, 2010.

620 Kuenen, J. G. and Robertson, L. A.: Ecology of Nitrification and Denitrification-Book.Pdf, in: *The Nitrogen and Sulphur*
621 *Cycles*, edited by: Cole, J. A. and Ferguson, S., Cambridge University Press, 162–218, 1987.

622 Kuypers, M. M. M., Silekers, A. O., Lavik, G., Schmid, M., Jørgensen, B. B., Kuenen, J. G., Sinninghe Damsté, J. S.,
623 Strous, M., and Jetten, M. S. M.: Anaerobic ammonium oxidation by anammox bacteria in the Black Sea, *Nature*, 422, 608–
624 611, <https://doi.org/10.1038/nature01472>, 2003.

625 Laffoley, D. and Baxter, J. M.: Ocean deoxygenation : everyone’s problem. Summary for policy makers,
626 <https://doi.org/10.2305/iucn.ch.2019.14.en>, 2019.

627 Lamb, A. L., Wilson, G. P., and Leng, M. J.: A review of coastal palaeoclimate and relative sea-level reconstructions using
628 $\delta^{13}\text{C}$ and C/N ratios in organic material, *Earth Sci Rev*, 75, 29–57, <https://doi.org/10.1016/j.earscirev.2005.10.003>, 2006.

629 Lembke-Jene, L., Tiedemann, R., Nürnberg, D., Gong, X., and Lohmann, G.: Rapid shift and millennial-scale variations in
630 Holocene North Pacific intermediate water ventilation, *Proc Natl Acad Sci U S A*, 115, 5365–5370,
631 <https://doi.org/10.1073/pnas.1714754115>, 2018.

632 Liu, Z., Altabet, M. A., and Herbert, T. D.: Glacial-interglacial modulation of eastern tropical North Pacific denitrification
633 over the last 1.8-Myr, *Geophys Res Lett*, 32, 1–4, <https://doi.org/10.1029/2005GL024439>, 2005.

634 Lu, Z., Hoogakker, B. A. A., Hillenbrand, C. D., Zhou, X., Thomas, E., Gutchess, K. M., Lu, W., Jones, L., and Rickaby, R.
635 E. M.: Oxygen depletion recorded in upper waters of the glacial Southern Ocean, *Nat Commun*, 48,
636 <https://doi.org/10.1038/ncomms11146>, 2016.

637 Lyle, M., Koizumi, I., Richter, C., Fox, P. J., Baldauf, J., and Francis, T. J. G.: Proceedings of the Ocean Drilling Program,
638 <https://doi.org/10.1097/BLO.0b013e3181576080>, 1997.

639 Matsumoto, K., Tanioka, T., and Rickaby, R.: Linkages between dynamic phytoplankton c:N:P and the ocean carbon cycle
640 under climate change, *Oceanography*, 33, 44–52, <https://doi.org/10.5670/oceanog.2020.203>, 2020.

641 Matul, A., Abelmann, A., Khusid, T., Chekhovskaya, M., Kaiser, A., Nürnberg, D., and Tiedemann, R.: Late Quaternary
642 changes of the oxygen conditions in the bottom and intermediate waters on the western Kamchatka continental slope, the Sea
643 of Okhotsk, *Deep Sea Res 2 Top Stud Oceanogr*, 125–126, 184–190, <https://doi.org/10.1016/j.dsr2.2013.03.023>, 2016.

644 Nicholson, S. E. and Flohn, H.: African climatic changes in late Pleistocene and Holocene and the general atmospheric
645 circulation., *Sea level, ice and climatic change. Proc. Canberra symposium, December 1979*, 2, 295–301, 1981.

646 Ortiz, J., Mix, A., Hostetler, S., and Kashgarian, M.: The California Current of the Last Glacial Maximum: Reconstruction at
647 42°N based on multiple proxies, *Paleoceanography*, 12, 191–205, <https://doi.org/10.1029/96PA03165>, 1997.

648 Paulmier, A. and Ruiz-Pino, D.: Oxygen minimum zones (OMZs) in the modern ocean, *Prog Oceanogr*, 80, 113–128,
649 <https://doi.org/10.1016/j.pocean.2008.08.001>, 2009.

650 Peng, X., Fuchsman, C. A., Jayakumar, A., Oleynik, S., Martens-Habbema, W., Devol, A. H., and Ward, B. B.: Ammonia
651 and nitrite oxidation in the Eastern tropical North Pacific, *Global Biogeochem Cycles*, 29, 2034–2049,
652 <https://doi.org/10.1002/2015GB005278>, 2015.

653 Peters, B., Horak, R., Devol, A., Fuchsman, C., Forbes, M., Mordy, C. W., and Casciotti, K. L.: Estimating fixed nitrogen
654 loss and associated isotope effects using concentration and isotope measurements of NO₃⁻, NO₂⁻, and N₂ from the Eastern
655 Tropical South Pacific oxygen deficient zone, *Deep Sea Res 2 Top Stud Oceanogr*, 156, 121–136,
656 <https://doi.org/10.1016/j.dsr2.2018.02.011>, 2018.

657 Pierce, S. D., Barth, J. A., Kipp Shearman, R., and Erofeev, A. Y.: Declining oxygen in the northeast Pacific, *J Phys*
658 *Oceanogr*, 42, 495–501, <https://doi.org/10.1175/JPO-D-11-0170.1>, 2012.

659 Placencia, J. A., Garcés-Vargas, J., Lange, C. B., and Hebbeln, D.: Alkenone-based temperature patterns along the eastern
660 South Pacific Coastal Ocean: the effect of upwelling and advection on the sedimentary alkenone unsaturation-index
661 (U37K'), *Biogeosciences Discussions*, 7, 545–564, 2010.

662 Rattray, J. E., Van De Vossenberg, J., Hopmans, E. C., Kartal, B., Van Niftrik, L., Rijpstra, W. I. C., Strous, M., Jetten, M.
663 S. M., Schouten, S., and Damsté, J. S. S.: Ladderane lipid distribution in four genera of anammox bacteria, *Arch Microbiol*,
664 190, 51–66, <https://doi.org/10.1007/s00203-008-0364-8>, 2008.

665 Rattray, J. E., Van Vossenberg, J. De, Jaeschke, A., Hopmans, E. C., Wakeham, S. G., Lavik, G., Kuypers, M. M. M.,
666 Strous, M., Jetten, M. S. M., Schouten, S., and Sinninghe Damsté, J. S.: Impact of temperature on ladderane lipid distribution
667 in anammox bacteria, *Appl Environ Microbiol*, 76, 1596–1603, <https://doi.org/10.1128/AEM.01796-09>, 2010.

668 Reid, J. L.: On the total geostrophic circulation of the pacific ocean : flow patterns , tracers , and transports, 39, 263–352,
669 1997.

670 Reid, J. L. and Mantyla, A. W.: On the Mid-Depth Circulation of the North Pacific Ocean, *J Phys Oceanogr*, 8, 946–951,
671 [https://doi.org/10.1175/1520-0485\(1978\)008<0946:otmdco>2.0.co;2](https://doi.org/10.1175/1520-0485(1978)008<0946:otmdco>2.0.co;2), 1978.

672 Robinson, R. S., Kienast, M., Albuquerque, A. L., Altabet, M., Contreras, S., Holz, R. D. P., Dubois, N., Francois, R.,
673 Galbraith, E., Hsu, T., Ivanochko, T., Jaccard, S., Kao, S., Kiefer, T., Kienast, S., Lehmann, M., Martinez, P., Mccarthy, M.,
674 Möbius, J., Pedersen, T., Quan, T. M., Ryabenko, E., Schmittner, A., Schneider, R., and Schneider-mor, A.: A review of
675 nitrogen isotopic alteration in marine sediments, 27, <https://doi.org/10.1029/2012PA002321>, 2012.

676 Rush, D. and Sinninghe Damsté, J. S.: Lipids as paleomarkers to constrain the marine nitrogen cycle, *Environ Microbiol*, 19,
677 2119–2132, <https://doi.org/10.1111/1462-2920.13682>, 2017.

678 Rush, D., Jaeschke, A., Hopmans, E. C., Geenevasen, J. A. J., Schouten, S., and Damsté, J. S. S.: Short chain ladderanes:
679 Oxidation products of anammox lipids, *Geochim Cosmochim Acta*, 75, 1662–1671,
680 <https://doi.org/10.1016/j.gca.2011.01.013>, 2011.

681 Rush, D., Wakeham, S. G., Hopmans, E. C., Schouten, S., and Sinninghe Damsté, J. S.: Biomarker evidence for anammox in
682 the oxygen minimum zone of the Eastern Tropical North Pacific, *Org Geochem*, 53, 80–87,
683 <https://doi.org/10.1016/j.orggeochem.2012.02.005>, 2012a.

684 Rush, D., Hopmans, E. C., Wakeham, S. G., Schouten, S., and Damst, J. S. S.: Occurrence and distribution of ladderane
685 oxidation products in different oceanic regimes, 2407–2418, <https://doi.org/10.5194/bg-9-2407-2012>, 2012b.

686 Rush, D., Hopmans, E. C., Wakeham, S. G., Schouten, S., and Sinninghe Damsté, J. S.: Occurrence and distribution of
687 ladderane oxidation products in different oceanic regimes, *Biogeosciences*, 9, 2407–2418, [https://doi.org/10.5194/bg-9-](https://doi.org/10.5194/bg-9-2407-2012)
688 2407-2012, 2012c.

689 Rush, D., Talbot, H. M., Van Der Meer, M. T. J., Hopmans, E. C., Douglas, B., and Damsté, J. S. S.: Biomarker evidence for
690 the occurrence of anaerobic ammonium oxidation in the eastern Mediterranean Sea during Quaternary and Pliocene sapropel
691 formation, *Biogeosciences*, 16, 2467–2479, <https://doi.org/10.5194/bg-16-2467-2019>, 2019.

692 Ryabenko, E.: Stable Isotope Methods for the Study of the Nitrogen Cycle, in: *Topics in Oceanography*, edited by:
693 Zambianchi, E., 49–88, <https://doi.org/10.5772/56105>, 2013.

694 Sahu, S., Allen, S. E., Saldías, G. S., Klymak, J. M., and Zhai, L.: Spatial and Temporal Origins of the La Perouse Low
695 Oxygen Pool: A Combined Lagrangian Statistical Approach, *J Geophys Res Oceans*, 127, 1–20,
696 <https://doi.org/10.1029/2021JC018135>, 2022.

697 Schneider, B., Schlitzer, R., Fischer, G., and Nöthig, E. M.: Depth-dependent elemental compositions of particulate organic
698 matter (POM) in the ocean, *Global Biogeochem Cycles*, 17, <https://doi.org/10.1029/2002gb001871>, 2003.

699 Sigman, D. M. and Fripiat, F.: Nitrogen isotopes in the ocean, in: *Encyclopedia of Ocean Sciences*, edited by: Kirk Cochran,
700 J., Bokuniewicz, H. J., and Yager, P. L., Elsevier Ltd, 263–278, <https://doi.org/10.1016/B978-0-12-409548-9.11605-7>, 2019.

701 Sinninghe Damsté, J. S., Strous, M., Rijpstra, W. I. C., Hopmans, E. C., Geenevasen, J. A. J., Van Duin, A. C. T., Van
702 Niftrik, L. A., and Jetten, M. S. M.: Linearly concatenated cyclobutane lipids form a dense bacterial membrane, *Nature*, 419,
703 708–712, <https://doi.org/10.1038/nature01067>, 2002.

704 Smith, K. L., Messié, M., Connolly, T. P., and Huffard, C. L.: Decadal Time-Series Depletion of Dissolved Oxygen at
705 Abyssal Depths in the Northeast Pacific, *Geophys Res Lett*, 49, <https://doi.org/10.1029/2022GL101018>, 2022.

706 Sollai, M., Hopmans, E. C., Schouten, S., Keil, R. G., and Sinninghe Damsté, J. S.: Intact polar lipids of Thaumarchaeota
707 and anammox bacteria as indicators of N cycling in the eastern tropical North Pacific oxygen-deficient zone,
708 *Biogeosciences*, 12, 4725–4737, <https://doi.org/10.5194/bg-12-4725-2015>, 2015.

709 Sonnerup, R. E., Quay, P. D., and Bullister, J. L.: Thermocline ventilation and oxygen utilization rates in the subtropical
710 North Pacific based on CFC distributions during WOCE, *Deep Sea Res 1 Oceanogr Res Pap*, 46, 777–805,
711 [https://doi.org/10.1016/S0967-0637\(98\)00092-2](https://doi.org/10.1016/S0967-0637(98)00092-2), 1999.

712 Stramma, L., Johnson, G. C., Firing, E., and Schmidtko, S.: Eastern Pacific oxygen minimum zones: Supply paths and
713 multidecadal changes, *J Geophys Res Oceans*, 115, 1–12, <https://doi.org/10.1029/2009JC005976>, 2010.

714 Tesdal, J. E., Galbraith, E. D., and Kienast, M.: Nitrogen isotopes in bulk marine sediment: Linking seafloor observations
715 with subseafloor records, *Biogeosciences*, 10, 101–118, <https://doi.org/10.5194/bg-10-101-2013>, 2013.

716 Thamdrup, B., Dalsgaard, T., Jensen, M. M., Ulloa, O., Farías, L., and Escribano, R.: Anaerobic ammonium oxidation in the
717 oxygen-deficient waters off northern Chile, *Limnol Oceanogr*, 51, 2145–2156, <https://doi.org/10.4319/lo.2006.51.5.2145>,
718 2006.

719 Thomson, R. E. and Krassovski, M. V.: Poleward reach of the California Undercurrent extension, *J Geophys Res Oceans*,
720 115, <https://doi.org/10.1029/2010JC006280>, 2010.

721 Thunell, R. C. and Kepple, A. B.: Glacial-Holocene D₁₅N record from the Gulf of Tehuantepec, Mexico: Implications for
722 denitrification in the eastern equatorial Pacific and changes in atmospheric N₂O, *Global Biogeochem Cycles*, 18,
723 <https://doi.org/10.1029/2002GB002028>, 2004.

724 Vallero, D. A.: Air pollution biogeochemistry, in: *Air Pollution Calculations*, edited by: Vallero, D. A., Elsevier, 175–206,
725 <https://doi.org/10.1016/b978-0-12-814934-8.00008-9>, 2019.

726 Verardo, D. J. and McIntyre, A.: AMERiA) I, 9, 63–86, 1994.

727 Vossenberg, J. Van De, Rattray, J. E., Geerts, W., Kartal, B., Niftrik, L. Van, Donselaar, E. G. Van, Damsté, J. S. S., Strous,
728 M., and Jetten, M. S. M.: Enrichment and characterization of marine anammox bacteria associated with global nitrogen gas
729 production, 10, 3120–3129, <https://doi.org/10.1111/j.1462-2920.2008.01643.x>, 2008.

730 Wang, Y., Hendy, I. L., and Zhu, J.: Expansion of the Southern California oxygen minimum zone during the early -to mid-
731 Holocene due to reduced ventilation of the Northeast Pacific, *Quat Sci Rev*, 238, 106326,
732 <https://doi.org/10.1016/j.quascirev.2020.106326>, 2020.

733 Ward, B. B.: How nitrogen is lost, *Science* (1979), 341, 352–353, <https://doi.org/10.1126/science.1240314>, 2013.

734 White, M. E., Rafter, P. A., Stephens, B. M., Wankel, S. D., and Aluwihare, L. I.: Recent Increases in Water Column
735 Denitrification in the Seasonally Suboxic Bottom Waters of the Santa Barbara Basin, *Geophys Res Lett*, 46, 6786–6795,
736 <https://doi.org/10.1029/2019GL082075>, 2019.

737 Whitney, F. A., Freeland, H. J., and Robert, M.: Persistently declining oxygen levels in the interior waters of the eastern
738 subarctic Pacific, *Prog Oceanogr*, 75, 179–199, <https://doi.org/10.1016/j.pocean.2007.08.007>, 2007.

739 Worne, S., Kender, S., Swann, G. E. A., Leng, M. J., and Ravelo, A. C.: Coupled climate and subarctic Pacific nutrient
740 upwelling over the last 850,000 years, *Earth Planet Sci Lett*, 522, 87–97, <https://doi.org/10.1016/j.epsl.2019.06.028>, 2019.

741 Yamamoto, M., Yamamuro, M., and Tanaka, Y.: The California current system during the last 136,000 years: response of
742 the North Pacific High to precessional forcing, *Quat Sci Rev*, 26, 405–414, <https://doi.org/10.1016/j.quascirev.2006.07.014>,
743 2007.

744 Zhou, Y., Gong, H., and Zhou, F.: Responses of Horizontally Expanding Oceanic Oxygen Minimum Zones to Climate
745 Change Based on Observations, *Geophys Res Lett*, 49, 1–11, <https://doi.org/10.1029/2022GL097724>, 2022.

746 Zonneveld, K. A. F., Versteegh, G. J. M., Kasten, S., Eglinton, T. I., Emeis, K., Huguët, C., and Koch, B. P.: Selective
747 preservation of organic matter in marine environments ; processes and impact on the sedimentary record, 483–511, 2010.

748

749